The Astrophysical Journal Supplement Series, 261:1 (17pp), 2022 July https://doi.org/10.3847/1538-4365/ac6c8f

BASS. XXI. The Data Release 2 Overview

Michael J. Koss[1,2], Benny Trakhtenbrot[3], Claudio Ricci[4,5], Franz E. Bauer[2,6,7], Ezequiel Treister[8], Richard Mushotzky[9], C. Megan Urry[10], Tonima T. Ananna[11], Mislav Baloković[12,13], Jakob S. den Brok[14,15], S. Bradley Cenko[16], Fiona Harrison[17], Kohei Ichikawa[18,19,20], Isabella Lamperti[21], Amy Lein[16], Julian E. Mejía-Restrepo[22], Kyuseok Oh[23,24,35], Fabio Pacucci[25,26], Ryan W. Pfeifle[27], Meredith C. Powell[28], George C. Privon[29,30], Federica Ricci[8,31], Mara Salvato[20], Kevin Schawinski[32], Taro Shimizu[20], Krista L. Smith[33], and Daniel Stern[34]

[1] Eureka Scientific, 2452 Delmer Street, Suite 100, Oakland, CA 94602-3017, USA; mike.koss@eurekasci.com
[2] Space Science Institute, 4750 Walnut Street, Suite 205, Boulder, CO 80301, USA
[3] School of Physics and Astronomy, Tel Aviv University, Tel Aviv 69978, Israel
[4] Núcleo de Astronomía de la Facultad de Ingeniería, Universidad Diego Portales, Av. Ejército Libertador 441, Santiago 22, Chile
[5] Kavli Institute for Astronomy and Astrophysics, Peking University, Beijing 100871, People's Republic of China
[6] Instituto de Astrofísica and Centro de Astroingeniería, Facultad de Física, Pontificia Universidad Católica de Chile, Casilla 306, Santiago 22, Chile
[7] Millennium Institute of Astrophysics (MAS), Nuncio Monseñor Sótero Sanz 100, Providencia, Santiago, Chile
[8] Instituto de Astrofísica, Facultad de Física, Pontificia Universidad Católica de Chile, Casilla 306, Santiago 22, Chile
[9] Department of Astronomy and Joint Space-Science Institute, University of Maryland, College Park, MD 20742, USA
[10] Yale Center for Astronomy & Astrophysics and Department of Physics, Yale University, P.O. Box 208120, New Haven, CT 06520-8120, USA
[11] Department of Physics and Astronomy, Dartmouth College, 6127 Wilder Laboratory, Hanover, NH 03755, USA
[12] Yale Center for Astronomy & Astrophysics, 52 Hillhouse Avenue, New Haven, CT 06511, USA
[13] Department of Physics, Yale University, P.O. Box 2018120, New Haven, CT 06520, USA
[14] Institute for Particle Physics and Astrophysics, ETH Zürich, Wolfgang-Pauli-Strasse 27, CH-8093 Zürich, Switzerland
[15] Argelander Institute for Astronomy, Auf dem Hügel 71, D-53231, Bonn, Germany
[16] Astrophysics Science Division, NASA Goddard Space Flight Center, Mail Code 661, Greenbelt, MD 20771, USA
[17] Cahill Center for Astronomy and Astrophysics, California Institute of Technology, Pasadena, CA 91125, USA
[18] Frontier Research Institute for Interdisciplinary Sciences, Tohoku University, Sendai 980-8578, Japan
[19] Astronomical Institute, Tohoku University, Aramaki, Aoba-ku, Sendai, Miyagi 980-8578, Japan
[20] Max-Planck-Institut für extraterrestrische Physik (MPE), Giessenbachstrasse 1, D-85748 Garching bei Müunchen, Germany
[21] Centro de Astrobiología (CAB), CSIC-INTA, Cra. de Ajalvir Km. 4, E-28850 Torrejón de Ardoz, Madrid, Spain
[22] European Southern Observatory, Casilla 19001, Santiago 19, Chile
[23] Korea Astronomy & Space Science institute, 776, Daedeokdae-ro, Yuseong-gu, Daejeon 34055, Republic of Korea
[24] Department of Astronomy, Kyoto University, Kitashirakawa-Oiwake-cho, Sakyo-ku, Kyoto 606-8502, Japan
[25] Center for Astrophysics | Harvard & Smithsonian, Cambridge, MA 02138, USA
[26] Black Hole Initiative, Harvard University, Cambridge, MA 02138, USA
[27] Department of Physics and Astronomy, George Mason University, 4400 University Drive, MSN 3F3, Fairfax, VA 22030, USA
[28] Kavli Institute of Particle Astrophysics and Cosmology, Stanford University, 452 Lomita Mall, Stanford, CA 94305, USA
[29] National Radio Astronomy Observatory, 520 Edgemont Road, Charlottesville, VA 22903, USA
[30] Department of Astronomy, University of Florida, P.O. Box 112055, Gainesville, FL 32611, USA
[31] Dipartimento di Fisica e Astronomia, Università di Bologna, via Gobetti 93/2, I-40129 Bologna, Italy
[32] Modulos AG, Technoparkstrasse 1, CH-8005 Zurich, Switzerland
[33] Department of Physics, Southern Methodist University, 3215 Daniel Avenue, Dallas, TX 75205, USA
[34] Jet Propulsion Laboratory, California Institute of Technology, 4800 Oak Grove Drive, MS 169-224, Pasadena, CA 91109, USA
Received 2021 September 7; revised 2022 April 29; accepted 2022 May 4; published 2022 July 15

Abstract

The BAT AGN Spectroscopic Survey (BASS) is designed to provide a highly complete census of the key physical parameters of the supermassive black holes (SMBHs) that power local active galactic nuclei (AGNs) ($z \lesssim 0.3$), including their bolometric luminosity ($L_{\rm bol}$), black hole (BH) mass ($M_{\rm BH}$), accretion rates ($L_{\rm bol}/L_{\rm Edd}$), line-of-sight gas obscuration ($N_{\rm H}$), and the distinctive properties of their host galaxies (e.g., star formation rates, masses, and gas fractions). We present an overview of the second data release of BASS (DR2), an unprecedented spectroscopic AGN survey in spectral range, resolution, and sensitivity, including 1449 optical (∼3200 Å–1 μm) and 233 near-IR (1–2.5 μm) spectra for the brightest 858 ultrahard X-ray (14–195 keV) selected AGNs across the entire sky and essentially all levels of obscuration. This release provides a highly complete set of key measurements (emission-line measurements and central velocity dispersions), with 99.9% measured redshifts and 98% BH masses estimated (for unbeamed AGNs outside the Galactic plane). The BASS DR2 AGN sample represents a unique census of nearby powerful AGNs, spanning over 5 orders of magnitude in AGN bolometric luminosity ($L_{\rm bol} \sim 10^{40}$–10^{47} erg s^{-1}), BH mass ($M_{\rm BH} \sim 10^{5}$–$10^{10}\,M_{\odot}$), Eddington ratio ($L_{\rm bol}/L_{\rm Edd} \gtrsim 10^{-5}$), and obscuration ($N_{\rm H} \sim 10^{20}$–$10^{25}$ cm^{-2}). The public BASS DR2 sample and measurements can thus be used to answer fundamental questions about SMBH growth and its links to host galaxy evolution and feedback in the local universe, as well as

[35] JSPS Fellow.

open questions concerning SMBH physics. Here we provide a brief overview of the survey strategy, the key BASS DR2 measurements, data sets and catalogs, and scientific highlights from a series of DR2-based works pursued by the BASS team.

Unified Astronomy Thesaurus concepts: Active galactic nuclei (16); AGN host galaxies (2017); X-ray active galactic nuclei (2035); X-ray surveys (1824); Sky surveys (1464); Supermassive black holes (1663)

1. Introduction

Although active galactic nuclei (AGNs) and the supermassive black holes (SMBHs) that power them have been studied for decades, there are still many key unresolved questions concerning the nature of these systems and how their evolution may be related to the galaxies that host them. While there are some clear SMBH–host correlations, such as the one between SMBH mass and bulge properties (Kormendy & Ho 2013) or the similar redshift evolution of star formation and SMBH growth (e.g., Heckman & Best 2014; Yang et al. 2019), it is not yet clear whether SMBH growth and AGN output (or "feedback," e.g., radiation, winds, jets) affects the host galaxy interstellar medium, star formation, and molecular gas (e.g., Fabian 2012). On smaller scales, it is not yet entirely clear what is the structure of the obscuring torus, what is its connection to its surroundings (e.g., Netzer 2015), and what is the role of obscuration by galaxy-scale gas and nuclear starbursts. Moreover, the stochasticity of SMBH fueling and consequent AGN emission (e.g., Hickox et al. 2014; Schawinski et al. 2015), combined with inherent biases in AGN survey techniques when identifying obscured AGNs (e.g., Hickox & Alexander 2018) make the connections between SBMH growth and feedback even less clear. Therefore, the only way to address the many open questions concerning SMBHs and AGNs, even in the local universe, and to construct statistically significant global trends and/or correlations is to have large samples (e.g., $N > 100$) surveyed with multiwavelength observations. Extragalactic hard (>2 keV) X-ray surveys provide one of the most complete ways to study growing black holes (BHs) in an unbiased way (see, e.g., Brandt & Alexander 2015; Brandt & Yang 2021). A large fraction, and indeed the majority, of the AGN population is obscured, and therefore the construction of a complete AGN census requires the identification of both obscured and unobscured sources (see review by, e.g., Hickox & Alexander 2018). At even higher energies, the ultrahard X-rays (>10 keV) provide a more complete tracer of the radiation for obscured AGNs ($N_{\rm H} > 10^{22}\,{\rm cm}^{-2}$) and even some Compton-thick (CT) AGNs ($N_{\rm H} > 10^{24}\,{\rm cm}^{-2}$; e.g., Ricci et al. 2015; Koss et al. 2016). An all-sky survey in the ultrahard X-ray band (>10 keV) thus provides an important way to answer the fundamental questions of SMBH growth and its links to host galaxy evolution, as well as many open questions concerning AGN physics, for a complete, unbiased sample of AGNs.

Over the past 20 yr, great progress has been made in surveying the ultrahard X-ray sky to increasing depths with the Burst Alert Telescope (BAT; Barthelmy et al. 2005) at 14–195 keV on board the the Neil Gehrels Swift Observatory (Gehrels et al. 2004) and the IBIS instrument (Ubertini et al. 2003) at 17–60 keV on board the INTEGRAL observatory (Winkler et al. 2003). Thanks to its wide field of view (FOV; 1.4 sr half coded), BAT monitors roughly 80% of the sky every day, providing regularly sampled average emission properties of objects. INTEGRAL/IBIS, with a roughly 13 times smaller FOV (0.11 sr half coded) but better angular resolution (12′ versus 19.′5 for BAT), has focused on targeting the Galactic plane and particularly the Galactic center region. Thus, the Swift BAT survey provides a uniform all-sky census of the average ultrahard X-ray emission of AGNs. Early analysis (e.g., Markwardt et al. 2005; Tueller et al. 2008) of the (ongoing) all-sky survey with BAT found that the brightest ultra-hard-X-ray-selected AGNs in the sky can probe nearby ($z < 0.1$) AGNs, including highly obscured systems; low-redshift, high-luminosity AGNs and quasars ($0.05 \lesssim z \lesssim 0.3$); and much more distant, beamed AGNs (reaching out to $z \gtrsim 3$). Specifically, the unbeamed BAT-detected AGNs span the moderate-to-high-luminosity end of the X-ray luminosity function (XLF; e.g., Maccacaro et al. 1991; Comastri et al. 1995; Gilli et al. 2007; Ueda et al. 2014; Aird et al. 2015; Buchner et al. 2015; Ananna et al. 2019) at all accessible redshifts, thus providing critical low-redshift templates for high-z sources detected in much deeper, pencil-beamed surveys (e.g., CDF-S, Luo et al. 2017; COSMOS, Civano et al. 2016). The low-redshift regime of the BAT AGN survey thus strongly complements high-redshift AGN surveys, providing a legacy data set with both high spatial resolution[36] and very high signal-to-noise ratio data obtained through relatively short observations. Finally, some AGNs are uniquely identified as AGNs in the hard X-rays (e.g., Smith et al. 2014). Other all-sky selection methods, such as WISE mid-IR (MIR) colors, are only able to uniformly classify the most luminous AGNs ($L^{\rm obs}_{2-10\,{\rm keV}} > 10^{44}\,{\rm erg\,s^{-1}}$; e.g., Ichikawa et al. 2017) owing to contamination from star formation in the host galaxies. Moreover, methods that use strong emission-line ratio diagnostics to identify AGNs (e.g., "BPT" Baldwin et al. 1981; Veilleux & Osterbrock 1987; Kewley et al. 2006) only select about half of the ultra-hard-X-ray-selected BAT AGNs (Koss et al. 2017). This is likely due to the contribution of star-forming regions in the AGN host galaxies (e.g., Koss et al. 2011a), combined with dust obscuration of the central, AGN-dominated line-emitting regions (e.g., Koss et al. 2010).

The ultimate goal of the BAT AGN Spectroscopic Survey (BASS) is to provide the largest available spectroscopic sample of Swift BAT ultrahard X-ray (14–195 keV) detected AGNs. BASS DR1 (Koss et al. 2017) used mostly archival optical spectra for 641 AGNs from the 70-month BAT catalog (Baumgartner et al. 2013). This was complemented by detailed 0.5–200 keV spectral measurements using Swift, Chandra, and XMM-Newton for 838 AGNs (Ricci et al. 2017a). A further 102 near-IR (NIR; 1–2.5 μm) spectra of BAT AGNs were reported on by Lamperti et al. (2017). Other data include high spatial resolution NIR adaptive optics (AO) imaging (Koss et al. 2018); extensive continuum modeling of the MIR and far-IR (FIR) emission from WISE, IRAS, Akari, and Herschel (Ichikawa et al. 2017, 2019); radio emission in several resolution regimes (Baek et al. 2019; Smith et al. 2020); and host-scale molecular gas measurements (Koss et al. 2021).

[36] The angular resolution at the median redshift $z = 0.04$ is 10× sharper than at $z = 1$, which is typical for deeper and narrower surveys.

From these data, numerous links and correlations were investigated, such as between X-ray emission and high-ionization optical lines (Berney et al. 2015), and/or ionized gas outflows (Rojas et al. 2020). A major result was the realization that the Eddington ratio is a key parameter in some of these links and scaling relations (e.g., Ricci et al. 2017b; Oh et al. 2017; Ricci et al. 2018). Other BASS DR1 studies focused on AGN clustering (Powell et al. 2018); the surprisingly weak (or indeed insignificant) correlation between the X-ray photon index, Γ, and Eddington ratio (Trakhtenbrot et al. 2017); the most luminous obscured AGNs (Bar et al. 2017); optically unobscured AGNs with massive X-ray absorbing columns (Shimizu et al. 2018); BAT blazars (Paliya et al. 2019); and a search for BH binaries (Liu et al. 2020). Since making BASS DR1 public, the BASS team has pursued additional optical and NIR spectroscopy toward the second data release of BASS (DR2), to obtain higher spectral resolution ($R \gtrsim 1500$) over the broadest possible spectral range (i.e., 3200–10000 Å), for the most complete sample of AGNs drawn from the 70-month BAT catalog. Below we present an overview of the BASS DR2, including a summary of our survey design and goals, data sets, key scientific results, and a comparison to other large AGN surveys. A more detailed, technical description of the DR2 observations and data is provided in Koss et al. (2022a). Throughout this work we adopt $\Omega_{\rm M} = 0.3$, $\Omega_{\Lambda} = 0.7$, and $H_0 = 70\ {\rm km\ s^{-1}\ Mpc^{-1}}$. To determine the extinction due to Milky Way foreground dust, we use the maps of Schlegel et al. (1998) and the extinction law derived by Cardelli et al. (1989).

2. Overview of DR2 Special Issue

BASS DR2 provides optical spectra and associated redshifts, broad and narrow emission line measurements, velocity dispersions, and derived quantities—particularly BH mass and Eddington ratio estimates—for a nearly complete (e.g., >95%) sample of the 858 AGN from the Swift BAT 70-month survey.

2.1. Major Science Goals and Key Measurements

The measurements and derived quantities provided through the BASS project are critical for the major science goals of the survey:

1. *Provide a (nearly) complete census of the brightest local AGNs from the unobscured to highly obscured*. Swift BAT, with its ultrahard X-ray sensitivity, serves as a primary discovery and survey tool for these local AGNs, as the energy range is uncontaminated by star formation and (nearly) unaffected by obscuration, and hence naturally provides a reliable tracer of AGN emission and SMBH growth within a volume-limited, highly complete survey.
2. *ConnectBH growth to their host galaxy properties to understand fueling and/or feedback*. It is critical to understand how the large range of SMBH-related properties—such as the bolometric luminosities, BH masses ($M_{\rm BH}$), accretion rates ($L_{\rm bol}/L_{\rm Edd}$), kinetic power of AGN-powered outflows and jets, and circumnuclear obscuration—relate to key host galaxy properties as traced by multiwavelength data, such as star formation rates (SFRs), stellar and molecular gas content, morphologies, and merger activity.
3. *Provide critical nearby templates for luminous high-redshift AGNs*. The BASS AGNs are local analogs of the powerful AGNs that form the bulk of the X-ray-detected population in deep pencil-beam surveys, where high spatial resolution (e.g., hundreds of parsecs) and sensitivity cannot be achieved.
4. *Provide critical diagnostics for rare and/or"abnormal" AGNs*. The unprecedentedly rich collection of multi-wavelength data collected for the BASS AGNs and its unique selection in the ultrahard X-rays allow one to identify, calibrate, and/or test selection criteria for highly obscured AGNs, highly accreting AGNs (i.e., $L_{\rm bol}/L_{\rm Edd} \gtrsim 1$), and other challenging subclasses, to be used with future facilities, surveys, and models.

2.2. Revised 70-month AGN Catalog

We briefly review the AGN catalog changes compared to BASS DR1, with further details provided in Koss et al. (2022a). The published 70-month BAT catalog (Baumgartner et al. 2013) is composed of 1210 ultrahard X-ray sources, including 822 classified as AGNs or associated with a galaxy and likely an AGN, 287 Galactic sources (e.g., high-mass X-ray binary, low-mass X-ray binary, cataclysmic variable, pulsar), 19 clusters, and 82 unknown sources. In the BASS DR1 (Ricci et al. 2017a, see Appendix A) new AGN candidates were identified among BAT detections based on WISE and soft X-ray data to increase the number of 70-month AGNs to 838.

However, even after the DR1, 44 unknown BAT sources, typically near the Galactic plane ($|b| < 10°$), had not been associated with counterparts. Of these sources, 22 were found to be AGNs. Fifteen of these unknown sources were subsequently identified as Galactic with NuSTAR and/or Chandra follow-up surveys (e.g., Yukita et al. 2017; Kennedy et al. 2020; Halpern et al. 2018) and/or based on optical spectroscopy obtained in the BASS/DR2 (see Koss et al. 2022a, for details). Another two sources that were classified as AGNs in the DR1 based solely on their hard X-ray spectra were found to be Galactic.

Unfortunately, their were still seven sources that lie very close to the Galactic plane ($|b| < 3°$) owing to their very high extinction values ($A_V \sim 5 - 43$ mag) and very high source confusion in the optical/NIR (i.e., multiple stars per 1 arcsec^2 area), which made optical and NIR spectroscopy of the counterpart impractical. The number of AGNs is 858 after these updates since two sources in the DR1 were discovered to be Galactic.[37]

For consistency with BASS DR1 and earlier studies, we classify AGNs according to the presence (or absence) of broad emission lines based on optical spectroscopy. Specifically, Sy1 are AGNs with broad Hβ line emission, Sy1.9 have narrow Hβ and broad Hα, while Sy2 AGNs have both narrow Hβ and narrow Hα (including small numbers of LINERs and AGNs in H_2-dominated regions). For beamed AGNs, the types include those with the presence of broad lines (BZQ), only host galaxy features lacking broad lines (BZG), or traditional continuum-dominated blazars with no emission lines or host galaxy features (BZB).

In addition to unbeamed AGNs, the Swift BAT survey includes also beamed and/or lensed AGNs, which are

[37] 838 DR1 AGNs − 2 DR1 AGNs found to be Galactic + 22 new AGNs = 858 DR2 AGNs + 7 unknown sources at $|b| < 3°$.

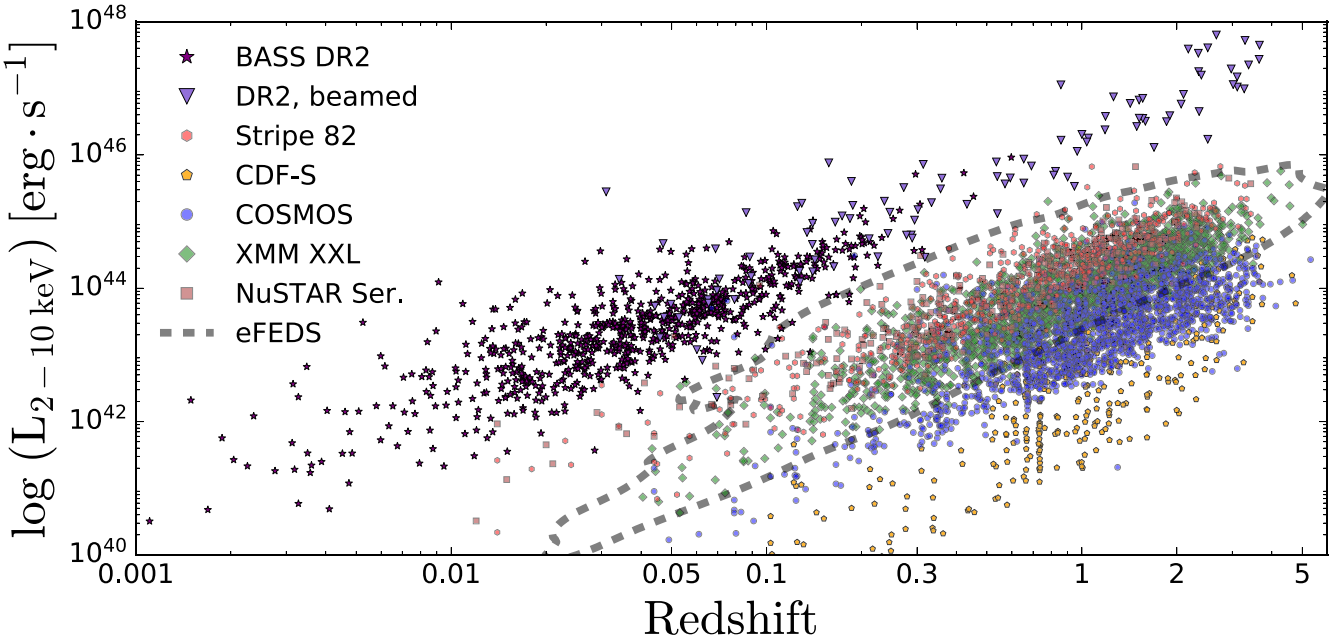

Figure 1. The rest-frame 2–10 keV luminosities of the BASS DR2 AGNs and of higher-redshift X-ray AGN surveys. Although BASS AGNs are selected based on their 14–195 keV emission, we plot the best-fit intrinsic 2–10 keV emission based on detailed X-ray spectral modeling (Ricci et al. 2017b). Unbeamed BASS AGNs are shown with purple stars, while beamed AGNs are shown with purple triangles. The unbeamed AGNs in the BASS sample tend to span the moderate-to-high-luminosity end of the XLF. We also show samples drawn from deeper X-ray AGN surveys, including Stripe 82X (red pentagons; LaMassa et al. 2016; Ananna et al. 2017), CDF-S (brown pentagons; Luo et al. 2017), Chandra COSMOS Legacy survey (blue circles; Civano et al. 2016; Marchesi et al. 2016), XMM XXL (green diamonds; Pierre et al. 2016), and the NuSTAR Serendipitous Survey (yellow squares; Lansbury et al. 2017). We also show contours for eFEDS containing 99% of the data (dashed gray; Salvato et al. 2022). We limit our comparison to X-ray sources with confirmed counterparts with spectroscopic redshifts. For eFEDS, unlike the other surveys, the soft-band flux (0.2–2.3 keV) was used to estimate the hard X-ray 2–10 keV emission assuming a power-law spectral model with $\Gamma = 1.7$ since only a small number of sources were detected above 2.3 keV (<1% Brunner et al. 2022). For these higher-redshift X-ray surveys we assumed a power-law spectral model with $\Gamma = 1.7$, to bring each X-ray luminosity to the rest frame by *K*-correcting the apparent luminosities based on the observed redshifts into the 2–10 keV rest frame. The deeper, higher-redshift samples tend to sample a luminosity range that is consistent with that covered by BAT, but at higher redshift.

important to separate for most scientific analyses. The DR2 has 105 beamed AGNs as identified by their multiwavelength emission, and particularly radio emission, and/or Gamma-ray emission detected by Fermi (e.g., Paliya et al. 2019). This includes both blazars, where the boosted continuum emission completely dominates the (rest-frame) UV/optical regime and no significant emission lines are seen, and flat-spectrum radio quasars (FSRQs), which do show broad emission lines (e.g., Paliya et al. 2019). There are additionally two lensed AGNs. One of the beamed AGNs (SWIFT J1833.7−2105, aka PKS 1830−211 at $z = 2.5$) is also lensed (Lidman et al. 1999)) by a foreground galaxy. Thus, the total sample of 858 includes 752 unbeamed AGNs, 104 beamed AGNs, 1 beamed and lensed AGN, and 1 lensed and unbeamed AGN.

An X-ray luminosity and redshift plot of the BASS DR2, with the newly revised redshifts and AGN classifications, is shown in Figure 1. The figure also shows a few other deep and narrow X-ray AGN surveys. We discuss these samples and their comparison in more detail in Section 5.3; however, it is clearly evident that BASS provides a natural low-redshift benchmark for distant surveys.

2.3. Survey Strategy and Observations

The sky distribution of all BASS DR2 optical spectroscopic observations is presented in Figure 2. Table 1 summarizes all of the BASS DR2 data, with further details provided in Koss et al. (2022a). The majority of the spectra used for the catalog measurements presented in DR2 papers come from either the Double Beam Spectrograph (DBSP) mounted on the Palomar Hale 5 m telescope (402 AGNs, mainly in the northern hemisphere) or the X-shooter spectrograph at the Very Large Telescope (VLT; 211 sources, mainly southern). In terms of DR2 spectroscopic targeting, our goals were to (1) provide the largest possible sample of BH mass measurements from either broad Balmer emission lines or stellar velocity dispersion measurements and (2) cover the broadest possible spectral range (e.g., 3200–10000 Å) for emission-line measurements, for the entire catalog of 858 AGNs. In practice, unless one uses echelle instruments (e.g., X-shooter), the latter goal requires either spectra with broad wavelength coverage and lower resolution or, alternatively, multiple, higher-resolution gratings and narrower wavelength coverage. The former goal motivates a spectral resolution of $R \gtrsim 1000$ ($\Delta v \lesssim 300\,\mathrm{km\,s^{-1}}$ for broad lines), and yet higher resolution (>2000) for stellar velocity dispersion measurements. Our targeting strategy was further complicated by the fact that for a significant number of targets we did not know a priori the broad/narrow-line nature of the sources, and thus whether high-resolution stellar velocity dispersion measurements were required. Repeated observations were therefore done if either the S/N of the broad Balmer lines (Hβ or Hα) or the S/N and/or spectral resolution of the stellar absorption features were too low. Repeated observations with higher spectral resolution but limited spectral range were primarily done for obscured AGNs (Sy1.9 and Sy2) to measure velocity dispersions (and deduce BH masses), as velocity dispersion measurements are much more difficult and less reliable for AGN-dominated continuum. We did not reobserve targets with acceptable spectra and measurements from the

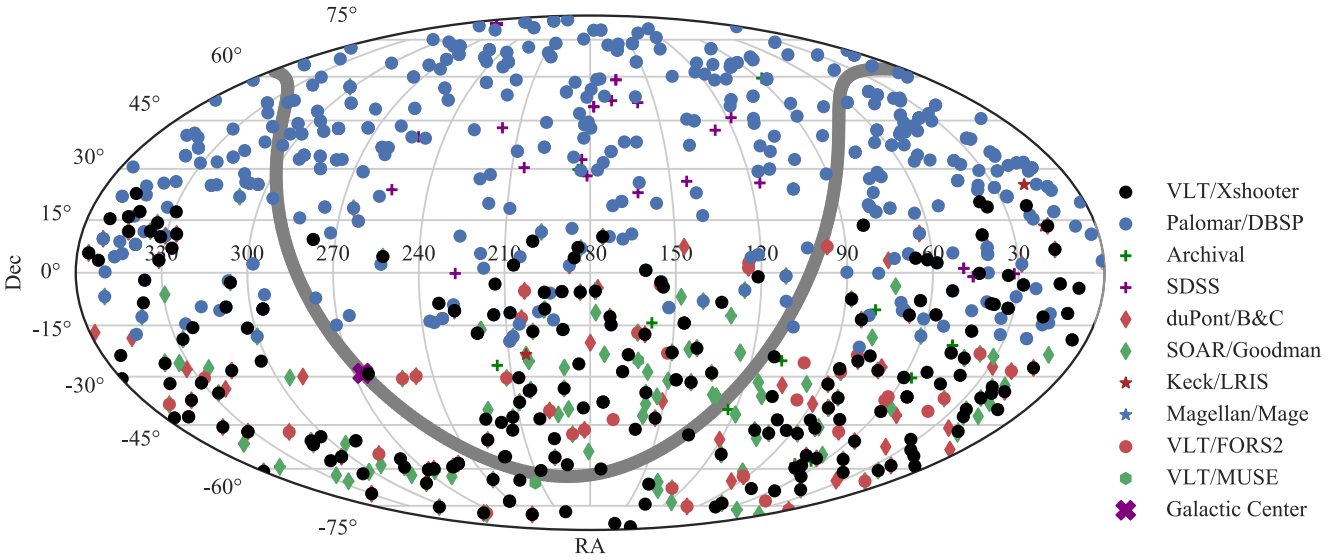

Figure 2. Overview of the BASS DR2 optical spectroscopy as observed on the sky (shown in equatorial coordinates and a Mollweide projection). The Galactic plane is indicated by the light-gray line.

Table 1
Summary of BASS DR2 Data

Telescope (1)	Instrument (2)	Total (3)	Range (Å) (4)	Slit Width (arcsec) (5)	R (6)
Palomar	DBSP	502	3150–10500	1.5	1220/1730
VLT	X-shooter	233	2990–10200	1.6/1.5	3850/6000
APO	SDSS	177	3830–9180	3	1760/2490
du Pont	BC	119	3000–9070	1	480
Archival[a]	Various	90	Various	Various	Various
VLT	FORS2	70	3400–6100	1	830
SOAR	Goodman	67	4560–8690	1.2	890/1630
Keck	LRIS	21	3200–10280	1	1280/1810
Magellan	MAGE	12	3300–10010	1	3850
VLT	MUSE	6	4800–9300	2	1850/3150
Velocity Dispersion Setups[b]					
SOAR	Goodman	86	7900–9070	1.2	4720
Palomar	DBSP	66	3970–5499/8050–9600	2	2170/4720
NIR DR2					
VLT	X-shooter	168	10240–24800	0.9	5400
Magellan	FIRE	65	8000–25000	0.6	6000

Notes. Column (1): telescope. Column (2): instrument. Column (3): total number of DR2 spectra observed with this setup. Column (4): wavelength range for the most common setup with the telescope. Columns (5)–(6): slit width and resolving power for the most common setup. In some cases larger or smaller slit widths (e.g., 1.″5 versus 2″) were used, resulting in different resolutions. See Koss et al. (2022a) for a detailed list of instrument setups. Two values are listed when the instrument had both a blue and red arm with different settings. Resolving power is wavelength dependent in some cases, and so the values are given at 5000 and 8500 Å depending on the spectral range.

[a] The archival sample is from earlier surveys that were not included in the DR1, including ROSAT AGNs that overlap with BASS in unpublished or published (Grupe et al. 2004) works, from the Palermo surveys of Swift BAT AGNs (Rojas et al. 2017), or as part of an atlas of low-redshift AGNs (Ho & Kim 2009). While not typically used in catalog measurements because of new DR2 data, we include these spectra for long-term studies of changing-look AGNs (e.g., MacLeod et al. 2019).

[b] These setups were done for velocity dispersion measurements of obscured AGNs (e.g., Sy1.9 and Sy2).

Sloan Digital Sky Survey (SDSS; York et al. 2000) included in Data Release 16 (DR16; Ahumada et al. 2020).

As the goal of BASS is to provide the best and most complete set of derived measurements (e.g., for narrow lines, broad lines, velocity dispersions), we did not require that all studies use the same single best spectra for an AGN in the DR2 as was done in the DR1. So for instance, a single Sy1.9 AGN may have a broad Hα measurement from SOAR/Goodman using the lower-resolution 400 line mm^{-1} setting, along with measurements of narrow emission lines, but have a velocity dispersion measurement from CaT using the 1200 line mm^{-1} setting. We also did not specifically exclude sources with high Galactic extinction if there was an obvious optical counterpart. This resulted in some spectra with very high extinctions

(between $A_V = 5$ and 10 mag) that are only suitable for basic emission-line identification/classification and for redshift measurement.

2.4. Comparison with BASS DR1

The BASS DR1 was composed mostly of past archival optical spectroscopic data from a variety of sources. Almost all the observations were from smaller (1.5–2.5 m) telescopes, with only 35 from the Palomar 5 m telescope (DBSP) and 29 from the 8.1 m Gemini North and South telescopes. Many of the spectra were taken from various surveys and studies that used various reduction routines, leading to substantial inhomogeneity in quality and parameter constraints. Some of the spectra, particularly those from the 6dF Galaxy Survey (6dFGS; Jones et al. 2009), had no proper flux calibration. Apart from the subset of DR1 spectra taken from the SDSS, most BASS DR1 spectra had a spectral resolution that is too low ($R < 1000$) to robustly measure stellar velocity dispersions. Finally, in most cases, the spectral setups did not include coverage below 4000 Å or beyond 7000 Å.

The DR2 results, which are based primarily on Palomar/DBSP or VLT/X-shooter spectra, are largely a separate release from DR1, even though the AGN samples overlap. Aside from 142 SDSS spectra commonly used for both samples, the only other spectral overlap between DR1 and DR2 is for 35 Palomar/DBSP observations, which were uniformly reprocessed in DR2 using the new `molecfit` (Smette et al. 2015) procedure for telluric corrections.

For the BASS DR2 catalogs of broad and narrow emission line measurements, we allowed some DR1 spectra to be used to have the best and most complete set of derived quantities (i.e., BH mass, etc.). This was done because the two main DR2 observing setups (VLT/X-shooter and Palomar/DBSP) used for the majority of sources both had the break in the blue and red CCDs at ∼5500 Å, making measurements of the spectral complex around the (redshifted) Hβ line problematic (e.g., at $z \approx 0.1$). For stellar velocity dispersion measurements, only DR2 data were used.

2.5. NIR DR2

The goal of the BASS NIR spectroscopy is to obtain wide spectral coverage across the full NIR range (∼1–2.4 μm) for a large sample of BAT AGNs. The 102 AGNs composing the NIR DR1 (Lamperti et al. 2017) were primarily for nearby AGNs ($z < 0.075$) observed with the SpeX instrument (Rayner et al. 2003) at the NASA Infrared Telescope Facility (IRTF) in the northern hemisphere (0.8–2.4 μm), along with archival Gemini/GNIRS data (0.8–2.5 μm). The NIR DR2 AGN sample includes 233 new NIR spectra of BASS AGNs. The new DR2 data were obtained from the southern hemisphere and include 168 new VLT/X-shooter (den Brok et al. 2022) and 65 Magellan/FIRE spectra (Ricci et al. 2022), both with substantially higher spectral resolutions ($R \sim 5000$–$10{,}000$) than the DR1 data ($R \sim 800$–1000). When including the NIR DR1, the total NIR sample provided as part of DR2 includes NIR spectroscopy of 322 unique AGNs.[38] The NIR catalog measurements include broad, narrow, and coronal emission line measurements between 1 and 2 μm, but not the K band (2–2.5 μm). The NIR spectroscopic survey of 322 AGNs is distinct from the DR2 optical spectroscopy, as it is an interim release rather than a complete sample (i.e., the NIR DR2 is very far from providing NIR spectra for all 858 AGNs in the optical BASS DR2). Moreover, this NIR survey release also includes some 105-month BAT sources (Oh et al. 2018), and the VLT/X-shooter spectroscopy only includes observations carried out through 2019 October. Future releases (i.e., the NIR DR3) will include additional NIR spectroscopy efforts within BASS that are currently ongoing, including additional VLT/X-shooter, Magellan/FIRE, and Palomar/TSpec observations, as well as velocity dispersion measurements and emission-line fitting in the K band (∼2–2.4 μm). As of 2021 July, an additional 267 BASS AGNs have NIR spectroscopy that are not part of the DR2 release.

2.6. Survey Uniformity and Completeness

BASS DR2 is nearly spectroscopically complete with respect to the 70-month BAT all-sky survey, with > 99% of the AGNs having spectra (i.e., 858/(858 AGNs+7 unknown/confused sources)). There are, however, some additional considerations in terms of uniformity and completeness for the BASS survey, which we briefly mention here and review in more detail in Koss et al. (2022a). The 70-month BAT survey reaches a 14–195 keV flux sensitivity level of 1.34×10^{-11} erg cm^{-2} s^{-1} over 90% of the sky (assuming a power-law spectral shape fixed to the Crab $\Gamma \sim 2.15$; Baumgartner et al. 2013) but 1.03×10^{-11} erg cm^{-2} s^{-1} over 50% of the sky, meaning that there is some small (∼20%) variation in sensitivity across the sky. Near the Galactic plane, and particularly in the crowded field of the Galactic center with strong Galactic X-ray background radiation, the source density is considerably lower, and the sensitivity of the BAT survey is a factor of two lower (Markwardt et al. 2005). The all-sky BAT survey also suffers from biases against harder and/or highly obscured AGNs. Due to the BAT detection method, which is calibrated to the Crab ($\Gamma = 2.15$), AGNs with harder intrinsic X-ray spectral energy distributions (SEDs; e.g., $\Gamma = 1.7$ vs. $\Gamma = 2.1$) will suffer roughly 10% reduced sensitivity (Koss et al. 2013). A more significant completeness correction is needed for highly obscured AGNs, where BAT detects 90% of the flux for an AGN with $N_H = 3 \times 10^{23}$ cm^{-2}, 50% for $N_H = 2 \times 10^{24}$ cm^{-2}, and ∼10% (or less, depending on models) at $N_H = 10^{25}$ cm^{-2} (e.g., Koss et al. 2016).

3. DR2 Papers, Catalogs, and Key Science Results

The DR2 papers listed in Table 2 provide a combination of large data sets of measurements and derived quantities, as well as scientific results for either the entire DR2 sample or considerable subsets of data. We provide a short review of these papers here, to explain the different measurements and catalogs provided in the various papers and to highlight key scientific findings. In some papers (e.g., narrow emission line measurements) a very wide spectral range was critical (3200–10000 Å), while in others (e.g., velocity dispersions) high spectral resolutions were critical; therefore, sometimes spectra with high spectral resolution but narrow wavelength range were used (e.g., for the calcium triplet, CaT, 8498, 8542, and 8662 Å). All DR2 spectra will be provided at the BASS website.[39]

[38] Four DR2 observations overlap with DR1, while nine DR2 Magellan/FIRE observations overlap with VLT/X-shooter.

[39] http://www.bass-survey.com

Table 2
Summary of BASS DR2 Papers

BASS No.	Short Title	Major Measurements/Science	Reference
XXI	Overview	M_{BH} and L_{bol}/L_{Edd} versus other surveys	This paper
XXII	Catalog	Counterparts, z, spectra, best M_{BH}	Koss et al. (2022a)
XXIII	MIR diagnostic for absorption	Obscuration in MIR	Pfeifle et al. (2022)
XXIV	Narrow-line measurements	BPT diagnostics	Oh et al. (2022)
XXV	Broad-line measurements	Sy 1-Sy 1.9 BLR versus N_H, broad lines	Mejía-Restrepo et al. (2022)
XXVI	Stellar velocity dispersions	Sy 1.9 and Sy 2 σ_* M_{BH}	Koss et al. (2022b)
XXVIII	NIR high-ionization and broad lines	NIR spectra, NIR lines	den Brok et al. (2022)
XXIX	NIR view of the BLR effects of obscuration	NIR BLR versus N_H	Ricci et al. (2022)
XXX	Distribution function of Eddington ratios	XLF, ERDF, BHMF	Ananna et al. (2022)

Note. List of all papers in the BASS DR2 release and associated major measurements and science. BASS XXVII was published separately from the DR2 release.

The main, detailed DR2 catalog paper (BASS XXII, Koss et al. 2022a) gives an updated list of counterparts and a complete summary of observing characteristics and reduction procedures for the 1449 optical spectra of the 858 AGNs from the BAT 70-month sample (Table 1). It discusses various issues for basic AGN observational studies (source confusion, chance alignment of multiple AGNs leading to flux boosting, dual AGNs, etc.), including a revised list of beamed and lensed AGN identifications. This paper also provides a set of overall best-derived measurements (e.g., redshifts and distances, bolometric luminosities, and M_{BH}) since multiple BH mass estimates are available for some sources from various tracers (i.e., different broad lines, velocity dispersions, and/or high-quality literature measurements). The overall best available measurements from this catalog are then used consistently in subsequent scientific papers. Narrow optical emission line measurements over the range 3200–10000 Å (e.g., [Ne V] λ3426, Hβ, [O III] λ5007, Hα, [N II] λ6583, [S III] λ9531) are presented in BASS XXIV (Oh et al. 2022). In that paper, we employ a full-range spectral fitting procedure, incorporating both stellar population synthesis models and empirical stellar templates, which deblends complex nebular emission-line features from the stellar components. We also study AGN subtypes as a function of X-ray column density; strong-line ratio diagnostic diagrams (BPT) and their links to Eddington ratio, and line width comparisons between X-ray BAT AGNs and optical SDSS AGNs. Broad emission line measurements (Hα, Hβ, Mg II λ2798, and C IV λ1549) and derived quantities are the focus of BASS XXV (Mejía-Restrepo et al. 2022). This paper includes virial estimates of BH mass (M_{BH}), which are used as the best BH mass measurement throughout DR2 and also allow estimates of the Eddington ratio (L_{bol}/L_{Edd}). The use of Mg II λ2798 and C IV λ1549 is reserved for the beamed AGNs with discernible broad lines, which are at higher redshifts (e.g., $z \gtrsim 1$), where rest-frame Hβ falls outside of the optical range. This paper concludes that the innermost part of the broad-line region (BLR), which contributes the highest velocity emission, is preferentially absorbed in obscured AGNs ($\log(N_H/\mathrm{cm}^{-2}) > 22$) and/or Sy1.9. This leads to a significant underestimation of the line flux compared to unobscured sources, which then strongly underestimates BH mass. These discrepancies typically exceed 1 dex and may reach 2 dex for heavily obscured AGNs ($\log(N_H/\mathrm{cm}^{-2}) \geqslant 24$). We provide some prescriptions for corrections.

Central velocity dispersion measurements (e.g., from [Ca H + K II$\lambda\lambda$3935, 3968, Mg I, or CaT regions) of obscured systems (Sy1.9 and Sy2) are investigated in BASS XXVI (Koss et al. 2022b). This paper finds that BASS AGNs have much higher velocity dispersions than the more numerous optically selected narrow-line AGNs (i.e., $\approx$150 vs. $\approx$100 km s^{-1}), but also that BASS AGNs are *not* biased toward the highest velocity dispersions seen in massive ellipticals (i.e., >250 km s^{-1}). Additionally, despite sufficient spectral resolution to resolve the velocity dispersions associated with the bulges of relatively small SMBHs ($\sim 10^4$–10^5 $M_\odot$), we do not find a significant population of such AGNs, which (given the BAT flux limit) would have presented super-Eddington accretion rates.

Ananna et al. (2022) use the highly complete set of BASS DR2 measurements to derive the intrinsic XLF, BH mass function (BHMF), and Eddington ratio distribution function (ERDF), for both obscured and unobscured low-redshift AGNs using the BAT sample. It employs an elaborate forward-modeling approach to derive the intrinsic XLF, BHMF, and BHMF from the observed distributions, while accounting for various selection effects. We find that the intrinsic ERDF of narrow-line (type 2) AGNs is significantly skewed toward lower Eddington ratios than those of broad-line (type 1) AGNs, while the BHMFs of these subsamples are consistent with each other. This result offers insights into the geometric structure of the obscuring "torus" and lends support to the radiation-regulated unification scenario (Ricci et al. 2017b), which suggests that radiation pressure dictates the geometry of the dusty obscuring structure around an AGN. The XLF, BHMF, and ERDF are also used to investigate the AGN duty cycle in the low-redshift universe.

Pfeifle et al. (2022) investigate the relationship between MIR colors and X-ray column density. Heavily obscured BAT AGNs are found to be more heavily X-ray suppressed, displaying lower ratios of $L^{obs}_{2-10\,keV}/L_{12\,\mu m}$, and they display "redder" MIR colors compared to unobscured AGNs. This paper develops diagnostic criteria that are designed to select both highly complete and highly reliable samples of heavily obscured AGNs ($\log(N_H/\mathrm{cm}^{-2}) > 23.5$). We also derive expressions relating the luminosity ratios and column density, to predict the AGN column density in lower count-rate X-ray SEDs, where detailed spectral modeling is impossible. These diagnostics could be used on future samples of AGNs, such as those being discovered by eROSITA (Predehl et al. 2021), to efficiently distinguish between heavily obscured and unobscured AGNs.

Den Brok et al. (2022) provide a detailed analysis of the NIR coronal lines (CLs; ionization potential $\chi > 100$ eV) and test their usage as indicators of AGN activity by comparing their strength, in particular that of [Si VI] λ19640, to the X-ray flux.

Table 3
Additional BASS and Archival Multiwavelength Data

Data Set/Telescope (1)	Spectral Bands (2)	N_{AGN} (3)	Focus (4)	Investigators (5)
NuSTAR	3–70 keV	527		Ricci, Koss, Archival
Swift XRT	0.5–10 keV	858		Ricci, Koss, Archival
XMM-Newton	0.5–10 keV	386		Ricci, Koss, Archival
Chandra	0.5–8 keV	384		Koss et al., Archival
Suzaku	0.3–10 keV	210		Archival
HST	F225W	54+	Sy1, $z < 0.1$	Koss et al.
Swift UVOT	UV ($W2$, $M1$, $W1$)/UBV	812		Ricci, Koss, Archival
XMM OM	UV ($W2$, $M1$, $W1$)/UBV	342		Ricci, Koss, Archival
SNIFS IFU	3200–10200 Å	46	$z < 0.05$	Koss et al.
MUSE IFU	4800–9300 Å	84		Archival
HST	F606W	157		Archival
HST	F814W	243	$z < 0.1$	Barth, Archival
HST	F160W	104		Archival
NIR AO (Keck/NIRC2, Gemini/GSAOI)	H, K	98+	$z < 0.1$	Koss, Treister et al.
NIR AO IFU (Keck/OSIRIS, VLT/SINFONI)	H, K	108+		Koss et al.
VLT/VISIR AO	8–13 μm	125	$z < 0.01$	Asmus et al.
Spitzer IRS low res.	5.3–35 μm	175		Archival
Spitzer IRS high res.	10–37 μm	140	$z < 0.05$	Weaver et al.
Herschel	70, 160, 250, 350, 500 μm	317	$z < 0.05$	Mushotzky, Shimizu et al.
JCMT/Scuba 2	450, 850 μm	63	$z < 0.05$	Koss et al.
ALMA	100 GHz	99		Archival
APEX/IRAM/JCMT	CO 1-0/CO 2-1	305+	z < 0.05	Koss, Shimizu, et al.
ALMA	CO 1-0/CO 2-1	156	<100 Mpc	Izumi et al., Archival
(J)VLA	22 GHz	232	$z < 0.05$	Smith, Mushotzky, et al.
VLBA	5 GHz	37	<40 Mpc	Secrest et al.
GBT	HI	96	$z < 0.05$	Winter et al.
ATCA/(J)VLA/WSRT/GMRT	HI mapping	98	<120 Mpc	Chung, Wong, et al.

Note. Column (1): telescope or instrument for the survey data. If the data are substantially similar (e.g., AO imaging in the same filter), we have grouped telescopes. Column (2): wavelength, frequency, line, filter, or energy band. Column (3): total number of unique AGNs from the Swift BAT 70-month catalog, which includes a total of 858 AGNs. This number does not include 105-month AGNs, which will be released in subsequent catalogs (BASS DRs). The plus sign indicates approved and/or ongoing additional observations. Column (4): indicates whether (part of) the observations were focused on a volume-limited sample and/or a particular AGN subclass. Column (5): main investigators for survey data. "Archival" indicates that the majority of corresponding data are from disparate observing programs.

A key finding is that CLs correlate more tightly (i.e., smaller scatter) with the X-ray fluxes than with the optical [O III] λ5007 line fluxes. Even in these bright AGNs, in only about half of the sources is a CL detected, limiting the extent to which CLs can be used as tracers of AGN activity. This study finds a clear trend of line blueshifts with increasing ionization potential in several CLs, such as [Si VI] λ19640, [Si X] λ14300, [S VIII] λ9915, and [S IX] λ12520, which elucidates the radial structure of the CL region.

Finally, Ricci et al. (2022) investigate the NIR BLR using Paα, Paβ, and He I λ10830 and associated virial BH mass estimates. The NIR regime is less affected by dust than the optical and can thus trace the innermost and fastest-moving BLR gas—even in the presence of mild obscuration. The study finds that the velocities of the BLR gas as estimated from the FWHMs of Hα and the NIR lines in Sy1–1.9 agree and are independent of the level of BLR extinction or obscuration (for $\log(N_H/\mathrm{cm}^{-2}) < 23.5$), but the broad-line luminosities are suppressed with increasing obscuration, biasing virial-based M_{BH} estimates. The latter finding is in agreement with the conclusion of Mejía-Restrepo et al. (2022; see above). The line luminosity decrement and the obscuration level at which it occurs change as a function of wavelength, with Hα experiencing a higher decrement than Paα (above $\log(N_H/\mathrm{cm}^{-2}) \simeq 21.0$ and 21.9, respectively). Thus, we caution against relying solely on Hα-based single-epoch BH mass estimates when $\log(N_H/\mathrm{cm}^{-2}) \gtrsim 21$ and on NIR lines when $\log(N_H/\mathrm{cm}^{-2}) \simeq 22$. A less biased proxy for the BLR radius in virial-based M_{BH} should be used at higher N_H, such as L_X.

4. Other BASS Observing Campaigns

Beyond the complete coverage with optical spectroscopy and the extensive NIR spectroscopy that are the main components of the BASS DR2, the BASS project aims to obtain and analyze large multiwavelength data sets for the BAT AGNs, in the X-ray, UV, optical, IR, FIR/submillimeter, and radio regimes. These include ongoing legacy BASS campaigns, past observations through BASS and the community, and various all-sky surveys (e.g., GALEX, GAIA, 2MASS, WISE, Akari, IRAS). The status of targeted observational programs for the 70-month AGNs as of 2021 July is summarized in Table 3 and on the BASS website.[40]

In addition to this, partial sky coverage exists from several wide-field surveys for hundreds of AGNs. Multiband high-quality optical imaging (<2″) exists for the majority (>80%) of BASS AGNs from the SDSS, the Panoramic Survey Telescope and Rapid Response System (Pan-STARRS; Chambers et al. 2016), the DESI Legacy Imaging Surveys (Dey et al. 2019), the VLT Survey Telescope ATLAS (Shanks et al. 2015), and targeted studies like Koss et al. (2011b). In the NIR, coverage

[40] http://www.bass-survey.com

exists in the VISTA Hemisphere Survey (VHS; McMahon et al. 2013) and the UKIRT Hemisphere Survey (UHS; Dye et al. 2018). In the radio, coverage at 1.4 GHz exists for more than half of the BAT AGNs (Wong et al. 2016) from the Faint Images of the Radio Sky at Twenty cm (FIRST; Becker et al. 1995) and NRAO VLA Sky Survey (NVSS; Condon et al. 1998).

The BAT AGNs have the largest coverage in the X-rays and UV, with all 858 observed with Swift/XRT and also observed with Swift/UVOT in the UV and optical. This results in a vast database of simultaneous X-ray and UV observations, obtained since the launch of Swift in 2004. For instance, for broad-line (Sy1) AGNs there are 32,184 distinct observations, due to the slewing nature of Swift and their intensive coverage in legacy observations of BAT AGNs.

As the brightest ultra-hard-X-ray-selected AGNs in the sky, many archival observations are available from several other X-ray telescopes. In particular, many BAT AGNs have also been observed as part of 20 ks filler observations in the NuSTAR BAT Legacy Survey,[41] which continues to observe approximately six BASS sources each month. A Chandra Cool Target program,[42] which started in 2019 January, is also observing nearby BAT AGNs ($z < 0.1$).

Another subset of observing programs focuses on high spatial resolution imaging ($\sim$100 pc) that can be achieved for nearby BASS AGNs ($z < 0.1$). This includes a recent HST SNAP program with the Advanced Camera for Surveys (ACS), which has obtained *i*-band (F814W) images for 154 DR1 BAT AGNs at $z < 0.1$ (Kim et al. 2021). A large HST SNAP program, approved through 2022, aims to obtain near-UV (<3000 Å) imaging of BASS AGNs, followed up with simultaneous X-ray and UV/optical observations of the nuclear AGN emission with Swift and ground-based optical imaging in *griz*. Koss et al. (2018) published 98 Keck/NIRC2 AO-assisted NIR observations (in the *Kp* band) for a volume-limited sample of AGNs ($z < 0.1$), along with many archival HST NIR observations of more nearby galaxies available from earlier HST/NICMOS studies (e.g., Hunt & Malkan 2004). Finally, approved high-resolution AO NIR imaging and spectroscopy are also underway through 2022 using Keck/NIRC2, Keck/OSIRIS, and Gemini/GSAOI, with a focus on hidden galaxy mergers and dual, small-separation AGNs in obscured systems.

Finally, another set of survey programs are broadly focused on connecting the key star-formation-related properties of the AGN hosts, such as SFR and molecular and atomic gas, with AGN activity in nearby AGNs, using high-resolution and high-sensitivity observations over the IR−millimeter−radio spectral regimes. These programs include earlier studies carried out with Spitzer (e.g., Weaver et al. 2010) and Herschel (e.g., Mushotzky et al. 2014), which focused on nearby BAT AGNs and were then followed up in the submillimeter and radio. The Herschel program to measure star formation observed 317 of the nearest BAT AGNs ($z < 0.05$), which were later followed up with more recent measurements of host galaxy molecular gas using CO lines (Koss et al. 2021) and 22 GHz (e.g., Smith et al. 2020) observations with the JVLA. A yet-nearer-distance sample ($z < 0.025$) is being targeted for HI mapping using the JVLA. More molecular gas observations using APEX have also been approved for these sources, through 2022. A program to obtain 100 pc resolution CO (2–1) measurements using ALMA was done for 33 nearby and luminous AGNs. High spatial resolution radio observations (0.2–0.5 pc resolution) that form a complete volume-limited sample out to 40 Mpc for AGNs above $L^{\rm obs}_{14-195\,\rm keV} > 10^{42}$ erg s^{-1} has also been done for a sample of 37 objects using C-band Very Long Baseline Array (VLBA).

[41] https://www.nustar.caltech.edu/page/legacy_surveys

[42] Chandra-BASS (C-BASS); https://cxc.harvard.edu/target_lists/CCTS.html.

5. Overall Survey Results

The BASS survey is spectroscopically complete for 100% (858/858) of the AGNs identified in the 70-month BAT all-sky survey outside of sources deep within the Galactic plane ($|b| < 3°$), which we were unable to target. The BASS DR2 reports redshifts for 99.9% (857/858) of the AGNs, excluding only one continuum-dominated blazar with a foreground Galactic star. This includes 47 redshifts reported for the first time. Outside of the Galactic plane ($|b| > 10°$), the survey completeness in BH mass measurements from broad lines or stellar velocity dispersion is 98% for all unbeamed AGNs because of the typically lower extinction in these regions. The remaining sources without BH mass measurements are mostly double-peaked and/or asymmetric broad-line AGNs and high-redshift Sy2 ($z > 0.1$), where high-quality velocity dispersion measurements are difficult. For beamed AGNs we report BH masses only for the BZQ class based on broad lines; for continuum-dominated blazars (BZB) velocity dispersion measurements are difficult due to the AGN-dominated continuum.

5.1. Survey Completeness and Measurables

In this section, we briefly illustrate the distributions of some of the key AGN-related properties of the BAT 70-month AGNs, as determined through the BASS DR2 measurements. We also briefly discuss the reliability and limitations of the measurements. A more elaborate forward-modeling approach accounting for various survey selection effects associated with a flux-limited survey with various levels of obscuration is described in Ananna et al. (2022).

Summaries of the typical bolometric luminosities, BH masses, Eddington ratios, and line-of-sight hydrogen column densities are provided in Tables 4 and 5 for unbeamed and beamed AGNs, respectively. Their BH mass versus Eddington ratio parameter space is shown in Figure 3. Overall, the completeness is quite similar for Sy1, Sy1.9, and Sy2 ($\sim$98%) outside the Galactic plane.

As a survey of the nearest and brightest hard-X-ray-selected AGNs in the sky, the measurement-associated uncertainties on BASS measurements are typically small. Apart from the beamed sources (e.g., blazars or "BZB") that lack emission lines and a handful of sources that are located in extremely crowded (Galactic plane) regions, the spectra of all BASS sources have multiple emission lines for robust redshift measurements. The uncertainties on BH mass determinations from σ_* are dominated by the systematics on the $M_{\rm BH}$–σ_* scaling relation (e.g., $\sim$0.3–0.5 dex; Marsden et al. 2020) rather than on the scatter found in repeat observations (Koss et al. 2022b; $\sim$0.1–0.2 dex). Similarly, the uncertainties on BH masses derived through spectral analysis of broad lines may reach $\sim$0.3–0.4 dex (Peterson 2014), whereas the measurement uncertainty is much lower (i.e., 0.1 dex; Mejía-Restrepo et al. 2022). The uncertainties on $N_{\rm H}$ are $\sim$0.05 dex for $\log(N_{\rm H}/{\rm cm}^{-2}) < 23.5$ and $\sim$0.3 for $\log(N_{\rm H}/{\rm cm}^{-2}) > 23.5$

Table 4
Summary of Unbeamed AGN Properties

Type	N	N $\lvert b\rvert > 10°$	z	$N_{M_{\rm BH}}$	$N_{M_{\rm BH}}$ $\lvert b\rvert > 10°$	% Meas. $M_{\rm BH}$	% Meas. $\lvert b\rvert > 10°$	log $M_{\rm BH}$ ($M_\odot$)	log $L_{\rm bol}$ (erg s^{-1})	log $L_{\rm bol}/L_{\rm Edd}$	log $N_{\rm H}$ (cm^{-2})
(1)	(2)	(3)	(4)	(5)	(6)	(7)	(8)	(9)	(10)	(11)	(12)
Sy1	359	318	0.050 ± 0.003	350	311	97	98	7.81 ± 0.04	44.87 ± 0.04	-1.17 ± 0.03	20.0 ± 0.05
Sy1.9	101	86	0.030 ± 0.004	97	84	96	98	7.98 ± 0.06	44.59 ± 0.08	-1.61 ± 0.09	22.28 ± 0.13
Sy2	292	259	0.029 ± 0.003	275	253	94	98	8.06 ± 0.04	44.50 ± 0.04	-1.71 ± 0.04	23.27 ± 0.05
Total	752	663	0.038 ± 0.002	722	648	96	98	7.96 ± 0.03	44.67 ± 0.03	-1.42 ± 0.03	21.98 ± 0.06

Note. Summary of the medians and standard error of the median for different populations of unbeamed AGNs. Column (1): AGN optical type based on the presence of broad Hβ and Hα. Column (2): total for the whole sample. Column (3): total excluding the Galactic plane region $|b| < 10°$, where high optical extinction makes measurements more difficult. Column (4): median redshift from optical lines. Columns (5)–(8): number of unique AGNs with $M_{\rm BH}$ measurements and excluding the Galactic plane region $|b| < 10°$, where high optical extinction makes measurements more difficult; also listed as percentages. Columns (9)–(12): median $M_{\rm BH}$, $L_{\rm bol}$, $L_{\rm bol}/L_{\rm Edd}$, and $\log(N_{\rm H}/{\rm cm}^{-2})$ for the sample.

Table 5
Summary of Beamed AGN Properties

Type	N	N, $\lvert b\rvert > 10°$	z	$N_{M_{\rm BH}}$	% Meas. $M_{\rm BH}$	log $M_{\rm BH}$	log $L_{\rm bol}$	log $L_{\rm bol}/L_{\rm Edd}$	log $N_{\rm H}$
(1)	(2)	(3)	(4)	(5)	(6)	(7)	(8)	(9)	(10)
BZQ	74	63	0.88 ± 0.12	67	91	8.83 ± 0.09	47.66 ± 0.16	0.38 ± 0.12	20 ± 0.11
BZB	22	18	0.13 ± 0.02				45.81 ± 0.12		20.57 ± 0.12
BZG	8	6	0.07 ± 0.02				45.11 ± 0.20		20.81 ± 0.11
Sy1/lensed	1	1	0.65	1	100	8.79	47.18	0.21	20
BZQ/lensed	1	0	2.51				49.49		22.77
Total	106	88	0.33 ± 0.10	68		8.83 ± 0.09	46.53 ± 0.14	0.38 ± 0.12	20.54 ± 0.08

Note. Summary of the medians and standard error of the median for different populations of beamed and/or lensed AGNs. Column (1): AGN optical type based on presence of broad lines (BZQ), only host galaxy features lacking broad lines (BZG), or traditional continuum-dominated blazars with no emission lines (BZB), or lensing. Column (2): total for the whole sample. Column (3): total excluding the Galactic plane region $|b| < 10°$, where high optical extinction makes measurements more difficult. Column (4): median redshift from optical lines. Columns (5)–(6): number of unique AGNs with $M_{\rm BH}$ measurements and percentages. Columns (7)–(10): median $M_{\rm BH}$, $L_{\rm bol}$, $L_{\rm bol}/L_{\rm Edd}$, and $\log(N_{\rm H}/{\rm cm}^{-2})$ for the sample.

(Ricci et al. 2017a). For intrinsic X-ray luminosity, the errors are typically < 0.1 dex (Lanz et al. 2019), unless the AGNs are CT, in which case the typical errors can reach ≈ 0.4 dex (Ricci et al. 2015). The bolometric luminosities are calculated from the intrinsic luminosities in the 14–150 keV range as shown in Ricci et al. (2017a, see their Table 12), using a bolometric correction of 8 (see, e.g., Koss et al. 2022a). In this case, the uncertainties are in the range of 0.2 dex (e.g., Trakhtenbrot et al. 2017).

We also looked at relationships between the line-of-sight column density, as measured from X-ray data, and BH mass and Eddington ratio, as determined from optical spectroscopy (Figure 4). One clear takeaway is that unobscured (Sy1) AGNs occupy a region of higher Eddington ratios compared to obscured (Sy1.9 and Sy2) AGNs. This echoes the previous BASS DR1–based finding by Ricci et al. (2017b), which supports a scenario where radiation pressure is the main driver of the geometry of the (dusty) circumnuclear gas. There are no obvious trends between $N_{\rm H}$ and either $M_{\rm BH}$ or $L_{\rm bol}/L_{\rm Edd}$ within each AGN optical subclass.

5.2. Redshift Survey Biases

Looking more carefully into Figure 3, the unbeamed BASS AGNs typically occupy narrow regions in the BH mass—Eddington ratio plane, in different redshift intervals. These could be easily understood as a combination of survey (flux) limits, AGN physics, and demographics. For example, the most distant AGNs in our sample ($z > 0.1$) include almost no sources with small BHs ($M_{\rm BH} \lesssim 10^7\ M_\odot$) because these would have to be super-Eddington to be detected.[43] Likewise, the lowest Eddington ratio sources ($L_{\rm bol}/L_{\rm Edd} \lesssim 10^{-3}$) are also almost exclusively at the highest-mass and lowest-redshift ($z < 0.01$) systems. However, while our sample is affected by strong low-mass and low accretion rate biases, there are no biases against super-Eddington non-beamed AGNs. Notably, such sources are extremely rare in the survey, suggesting that the Eddington limit remains meaningful despite the simplifications in its derivation.[44]

We show the Eddington ratio versus redshift in the top panel of Figure 5. Despite the aforementioned possible biases, Sy1 sources tend to have higher Eddington ratios (on average) than Sy1.9 or Sy2 sources, even when matched in redshift, though this difference decreases toward the highest redshifts in the sample ($z > 0.05$). The Sy1.9 and Sy2 classes follow the same distribution in $L_{\rm bol}/L_{\rm Edd}$ rising sharply with redshift from $L_{\rm bol}/L_{\rm Edd} \approx 10^{-2}$ at $z = 0.01$ to $L_{\rm bol}/L_{\rm Edd} \approx 6 \times 10^{-2}$. Conversely, the median Eddington ratio of Sy1 galaxies is nearly flat with redshift ($L_{\rm bol}/L_{\rm Edd} \approx (7-9) \times 10^{-2}$).

[43] That is, $L_{\rm bol} \propto M_{\rm BH} \times L_{\rm bol}/L_{\rm Edd}$ for a high-z source would result in a low flux.

[44] The alternative is that super-Eddington accretion in SMBHs is extremely X-ray weak (e.g., Laurenti et al. 2022).

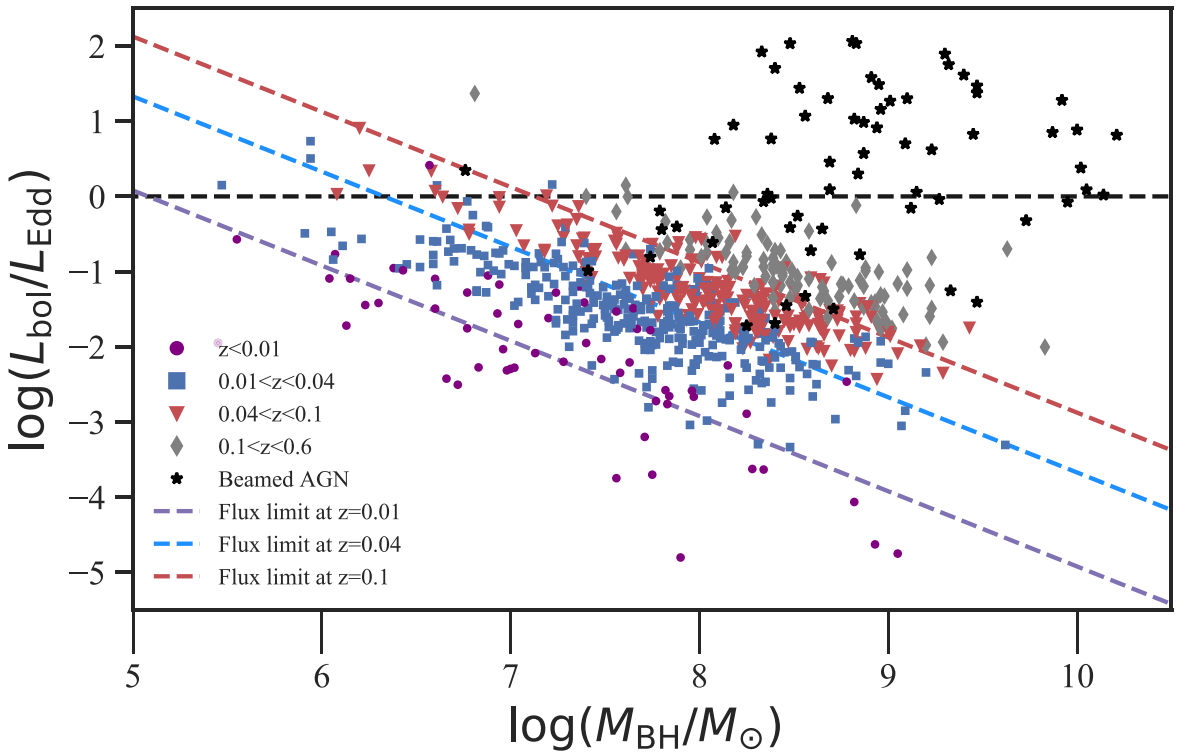

Figure 3. Distribution of BH masses ($M_{\rm BH}$) and Eddington ratios ($L_{\rm bol}/L_{\rm Edd}$) for the entire sample of BASS AGNs for which redshift measurements are available, including unbeamed AGNs (e.g., Sy1, Sy1.9, and Sy2) and beamed AGNs (BZQs). The lower limits on $M_{\rm BH}$ and $L_{\rm bol}/L_{\rm Edd}$ due to the survey flux limits are illustrated with dashed (antidiagonal) lines, for various redshifts corresponding to $z = 0.01$ ($L_{\rm bol} = 1.8 \times 10^{43}$ erg s^{-1}), $z = 0.04$ ($L_{\rm bol} = 3.2 \times 10^{44}$ erg s^{-1}), and $z = 0.1$ ($L_{\rm bol} = 2.0 \times 10^{45}$ erg s^{-1}). Errors in $M_{\rm BH}$ are of order 0.5 dex owing to systematic uncertainties in virial and σ_*-based scaling relations (e.g., Ricci et al. 2022). The BASS unbeamed AGNs occupy narrow, redshift-dependent slices of the $M_{\rm BH} - L_{\rm bol}/L_{\rm Edd}$ plane owing to the Eddington limit and survey flux limits (see text for details). Interestingly, we find that the $\log(L_{\rm bol}/L_{\rm Edd})$ tends to be bounded at -2.5 to -3, possibly associated with BAT identifying disk accretion primarily rather than inefficient accretion and the upper bounds at the Eddington limit (except for beamed AGNs). The lower bound of the BH mass distribution corresponds to $\log(M_{\rm BH}/M_\odot) = 5$, where the range pushes into intermediate-mass BHs and would only be sensitive to Eddington/super-Eddington accretion, if it exists. The upper limit at $\log(M_{\rm BH}/M_\odot) = 10$ is largely due to the space density of massive BHs.

5.3. Comparison to Other Surveys

A comparison to other distant AGN X-ray surveys is shown in Figure 1. Due to its all-sky coverage, the BAT AGNs include the highest number of sources at $z < 0.1$, the most luminous unbeamed QSOs at $0.1 < z < 0.6$, and a population of high-redshift beamed AGNs between $z = 1$ and 3.5. In luminosity space the survey overlaps well with medium-deep surveys (e.g., XMM XXL, Stripe 82, and COSMOS) at $0.5 < z < 3$.

Among all-sky X-ray surveys, it is useful to compare the BAT AGNs to the past ROSAT survey in the soft X-ray band (0.1–2.4 keV; Truemper 1982). The more recent reprocessing of the second ROSAT all-sky survey (2RXS) source catalog (Boller et al. 2016) had a flux limit of $\sim 10^{-13}$ erg cm^{-2} s^{-1} at 0.1–2.4 keV, with ~130,000 sources. Assuming $\Gamma = 1.8$, this flux limit corresponds to $\sim 2 \times 10^{-13}$ over the BAT 14–195 keV band, which is ~50× deeper than the 70-month BAT survey. Of these, 7005 ROSAT sources were cross-matched with the SDSS Data Release 5 (Anderson et al. 2007). Due to the soft X-ray sensitivity of ROSAT, the vast majority of these sources (6224/7005, or 89%) were broad-line AGNs, whereas the fraction within BASS for such (unbeamed) sources is 42%. In addition, the median redshift of the (subset of) ROSAT sources was $z = 0.42$, which is more than a factor of 10 more distant than the unbeamed BASS AGNs ($z \simeq 0.037$). The BASS overlap with ROSAT is 95% for Sy1 sources, down to 53% for Sy2, and only 30% for LINERs (see, e.g., Oh et al. 2022, for further details). A more comprehensive comparison between the 2RXS and the BAT AGNs is also available in Oh et al. (2018).

The concurrent eROSITA mission and its all-sky survey (0.2–8 keV; Predehl et al. 2021) are expected to eventually yield a few million AGNs and be roughly a factor of 100 times deeper ($\sim 10^{-15}$ erg cm^{-2} s^{-1}) than ROSAT, which means a particularly larger number of higher-redshift sources. The eROSITA Final Equatorial Depth Survey (eFEDS), with a depth of $\sim 10^{-14}$ erg cm^{-2} s^{-1} at 0.5–2 keV (Wolf et al. 2021) over 140 deg^2, provides some early insight into what one could expect for the AGN population to be surveyed by eROSITA. Specifically, 90% are unobscured ($\log(N_{\rm H}/{\rm cm}^{-2}) < 21.5$), and the redshift distribution peaks at around $z \simeq 1$ (Liu et al. 2022), though redshift determination for the majority of sources is problematic until larger spectroscopic surveys are completed (e.g., via SDSS-V, Kollmeier et al. 2017; and/or VISTA/4MOST, Salvato et al. 2022). Thus, we expect that BASS will provide a bright complement of well-understood luminous nearby sources ($z \simeq 0.037$) that is less biased with regard to obscuration, but also missing the numerous distant AGNs to be detected by eROSITA.

To put the BASS sample in perspective, we also compare it to several other optical surveys of nearby luminous AGNs, including the SDSS quasars (Shen et al. 2011), SDSS Sy2 AGNs (Greene & Ho 2005), PG quasars (Boroson & Green 1992), and type 2 quasars selected using [O III] λ5007 emission (Kong & Ho 2018). Compared to these samples, the

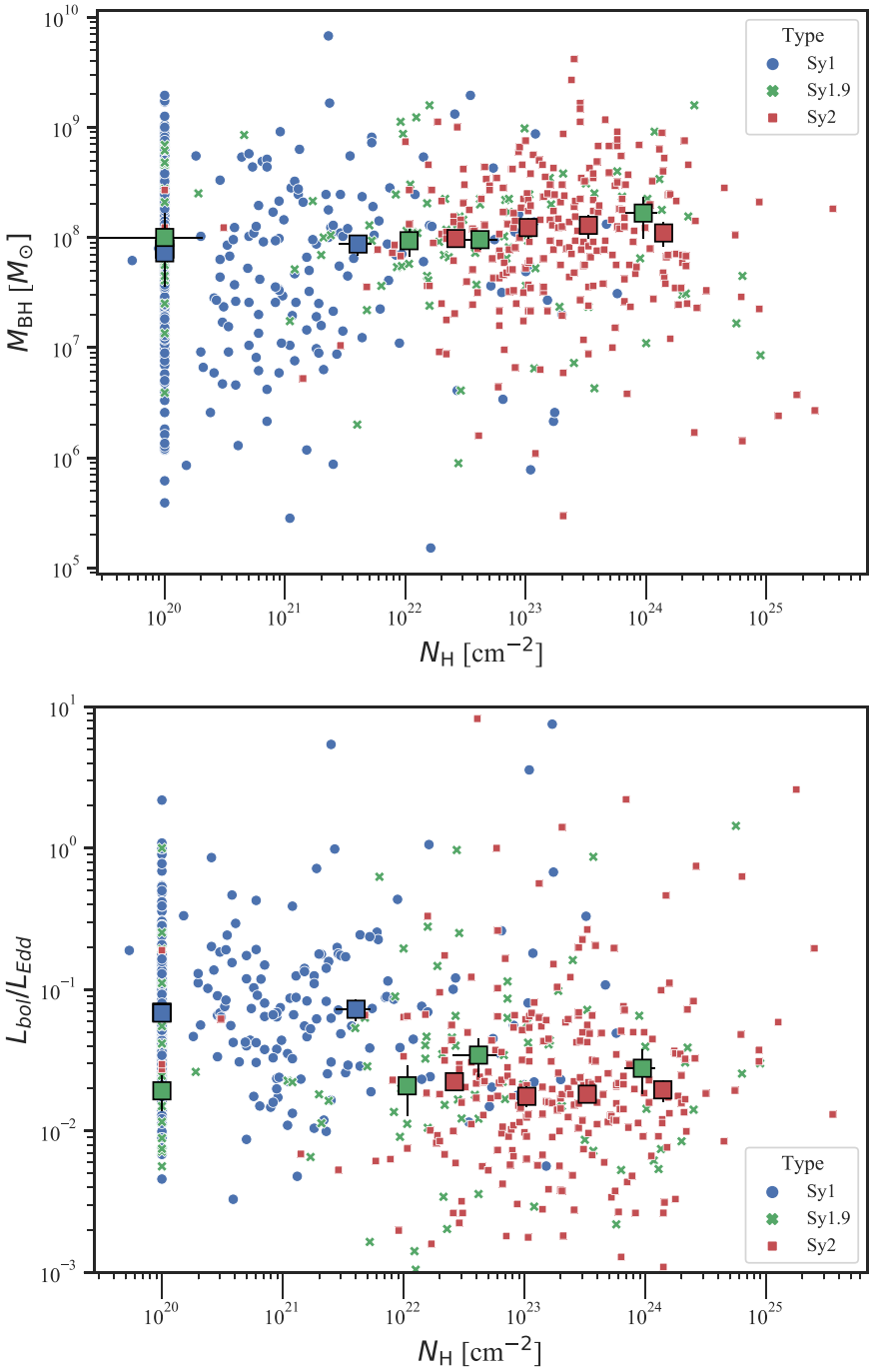

Figure 4. Summary scatter plots of the line-of-sight hydrogen column density (N_H, an obscuration indicator) vs. BH mass (top) and Eddington ratio (bottom). Different symbols mark subclasses of unbeamed BASS AGNs (e.g., Sy1, Sy1.9, and Sy2). X-ray measurements of $N_H = 10^{20}$ cm^{-2} are essentially upper limits and represent sources with no sign of obscuration. The large squares indicate the binned medians for each subclass. Error bars on the plotted median values are equivalent to 1σ and calculated based on a bootstrap procedure with 100 realizations. The bin sizes were constructed to have equal numbers of sources in each bin. The Sy1 AGNs tend to have higher Eddington ratios than the narrow-line AGNs (Sy1.9 and Sy2). Typical 90% errors in N_H are <0.2 dex based on X-ray modeling (Ricci et al. 2017a), but higher for heavily obscured AGNs, log log(N_H/cm^{-2}) > 24.5.

BAT-selected AGNs are typically found at lower redshifts ($z < 0.1$). The Eddington ratios of broad-line (Sy1) AGNs are above the SDSS Sy2 AGNs, consistent with those of SDSS and PG quasars, but below the SDSS type 2 quasars. Among Sy1.9 and Sy2 types, only the highest-redshift BAT sources ($z > 0.08$) have similar Eddington ratios to the SDSS quasars and PG quasars. However, the SDSS type 2 quasars tend to have significantly higher Eddington ratios than BAT Sy1.9 or Sy2 types, despite overlap in redshift at $z = 0.1$. Finally, BASS Sy2 galaxies tend to have higher Eddington ratios than SDSS Sy2 galaxies.

The most luminous quasars in our sample are generally not found in other quasar samples. We investigated whether the most luminous BAT AGNs were selected by the SDSS quasars and type 2 quasar samples and found virtually no BAT AGNs in these samples. We focused specifically on the range of

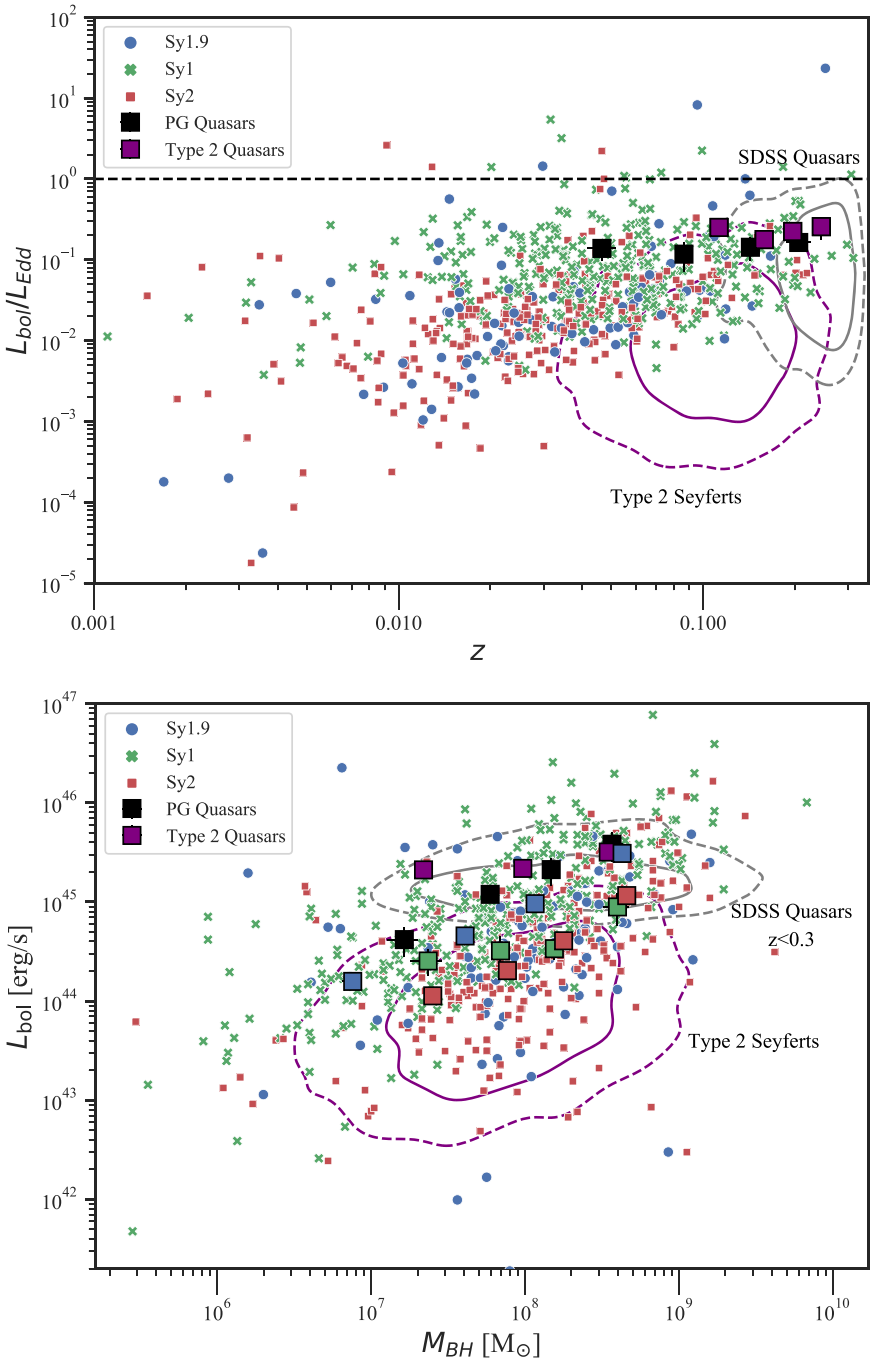

Figure 5. The distribution of BASS DR2 AGNs in the Eddington ratio vs. redshift (top) and bolometric luminosity vs. BH mass (bottom) planes. The large squares indicate the binned medians for each AGN subclass with redshift (top) and $M_{\rm BH}$ (bottom). Error bars on the plotted median values are equivalent to 1σ, calculated based on a bootstrap procedure with 100 realizations. The number of bins was fixed to four constructed to have equal numbers of sources in each bin. For comparison, we plot SDSS quasars at $z < 0.3$ (gray contours; Shen et al. 2011) and lower-luminosity SDSS type 2 Seyferts (purple contours; Greene & Ho 2005). The solid and dashed contours cover 68% and 95% of the data, respectively. We also plot the median for PG quasars (Boroson & Green 1992; black squares) and SDSS type 2 quasars (Kong & Ho 2018) selected based on their [O III] λ5007 emission (purple squares). The BASS AGNs have roughly similar BH masses and bolometric luminosities to the different SDSS samples but also extend to lower redshifts and BH masses. We note that there is essentially no overlap between BASS DR2 and these SDSS-based samples of powerful AGNs (see text for discussion).

$z < 0.3$ and $L_{\rm bol} > 10^{46}$ erg s^{-1}, which includes 18 unbeamed BAT AGNs, of which 8 are found within the SDSS footprint. Of these, only one source (SWIFT J1547.5+2050, aka 3C 323.1) is selected by the SDSS quasar sample. The other seven AGNs were not targeted for SDSS spectroscopy. In five cases the quasar is classified as a star in terms of colors, and in two cases the obscured (Sy2) AGNs are classified as galaxies, but no spectra were taken.

On the other hand, there are 14 SDSS quasars with $L_{\rm bol} > 10^{46}$ erg s^{-1}, which are not detected by the BAT survey. The BAT detection limit at $z = 0.3$ for 90% sky coverage is equivalent to $L_{\rm bol} = 1.1 \times 10^{46}$ erg s^{-1}, assuming a simple

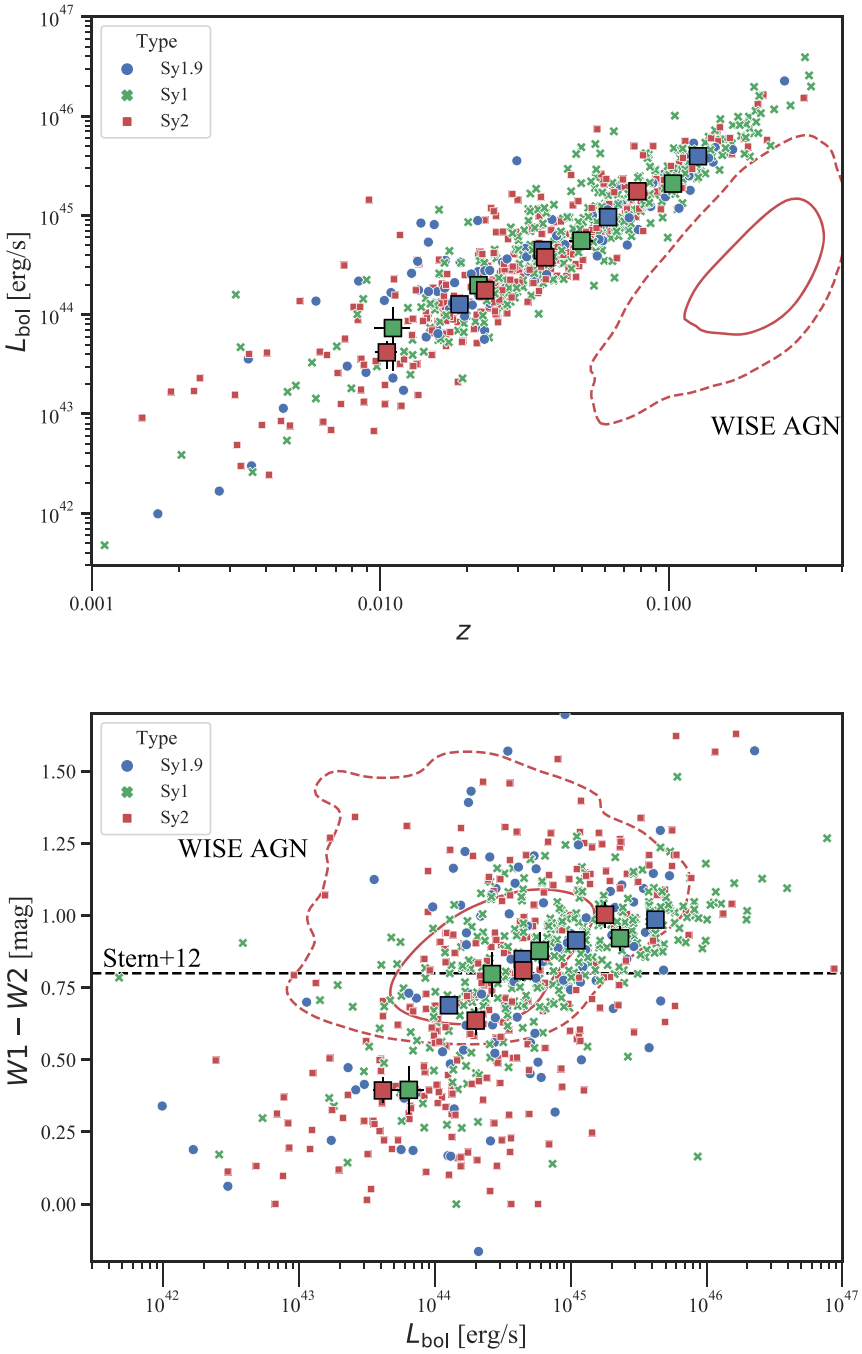

Figure 6. The distribution of BASS DR2 in the bolometric luminosity vs. and redshift (top) and WISE colors vs. bolometric luminosity (bottom) planes. For comparison, we also plot the distributions of WISE-selected AGNs at $z < 0.3$ (Assef et al. 2018; red contours), with SED fitting and redshifts measured from the SDSS (Barrows et al. 2021). The solid and dashed contours cover 68% and 95% of the WISE AGN data, respectively. A black dashed line indicates the WISE color cut to identify AGNs (W1 − W2 > 0.8; Stern et al. 2012). The BAT AGNs tend to probe similar luminosities to the higher-redshift WISE AGNs, but at lower redshifts.

conversion of $L_{bol} = 8 \times L^{obs}_{14-195\ keV}$ erg s^{-1} (e.g., Koss et al. 2017). Hence, all 14 SDSS quasars should be detected. It is possible that these undetected quasars may be part of a class of X-ray-weak quasars that have been found by several campaigns (e.g., Laor et al. 1997; Pu et al. 2020). Alternatively, the single, constant X-ray bolometric correction, rather than a luminosity-dependent one (e.g., Duras et al. 2020), may be too low for our sample. Techniques can be used to study known sources at $\sim$3 $\times$ fainter limits within BAT and would be ideal for this population (e.g., Koss et al. 2013). We reserve further discussion for future detailed studies. For the SDSS type 2 quasars, there is no overlap between the samples, with 26 AGNs in the type 2 quasars having $L_{bol} > 10^{46}$ erg s^{-1} and 0/26 detected by BAT, when all should be detected.

We further compare the bolometric luminosities and BH masses of the BASS DR2 sample. Only the most luminous quartile of Sy1.9 and Sy2 AGNs reaches the average luminosities of the SDSS quasars at similar redshifts ($z < 0.3$). By comparison, roughly half of the BASS Sy1 sample occupies similar distributions in bolometric luminosity

and BH mass to those of the SDSS quasars. The Sy1 galaxies have similar luminosities to the PG quasars, other than the least luminous quartile, but somewhat larger BH masses. The SDSS type 2 quasars occupy a region significantly above the BAT Sy1.9 and Sy2 galaxies in $L_{\rm bol}$, reached only by the most luminous quartile of the Sy1 galaxies.

Finally, the BASS sample has a significant number of low-mass BHs ($M_{\rm BH} < 10^7\,M_\odot$) that are not present in any of the other comparison samples. This feature of BASS is due to the higher spectral resolution ($R > 2500$) in the optical spectroscopy, which allows us to resolve spectral features tracing smaller BHs; the purely AGN-dominated selection in the >14 keV band, which allows us to study low-$M_{\rm BH}$ AGNs whose optical emission is host dominated; and the ability to study even the nearest AGNs (i.e., $z < 0.01$) that are saturated in SDSS imaging and thus excluded from the spectroscopic follow-up. A small number of nearby ($z < 0.01$) SMBHs have Eddington ratios as low as $\simeq 10^{-5}$ (e.g., M81; Devereux 2019) and offer an opportunity to study the emission properties of advection-dominated accretion flows (Yuan & Narayan 2014). These radiatively inefficient accretion flows result in broadband SEDs that are markedly different from those characterizing standard, thin-disk accretion (see, e.g., Ryan & MacFadyen 2017).

We finally compare the BASS DR2 sample to MIR-selected AGNs. The standard WISE color cut ($W1 - W2 > 0.8$; Stern et al. 2012) identifies only 56% of the BAT AGN sample (482/858). The fraction of detections is highly dependent on AGN luminosity, with a much higher fraction of luminous AGNs detected (Figure 6; see also Ichikawa et al. 2017).

We also compare the number of BASS AGNs in the WISE-selected AGNs drawn from the 30,093 deg^2 of extragalactic sky in the AllWISE Data Release (Assef et al. 2018). The AllWISE AGN study by Assef et al. (2018) provides an AGN catalog with 90% reliability (the "R90" catalog), selected purely using the WISE W1 and W2 bands, but with lower completeness. However, many of the BAT AGNs are excluded by default because they reside in galaxies that are extended in the Two Micron All Sky Survey (2MASS), a criterion adopted by the WISE AGN catalog to avoid contamination by separate, resolved parts of nearby galaxies. We find that only about 74/858 BASS DR2 sources overlap with the WISE R90 AGN catalog (9%), including 37 broad-line AGNs (Sy1–1.8), 6 narrow-line AGNs (Sy1.9–2), 28 beamed broad-line AGNs, and 3 continuum-dominated blazars (BZB). This corresponds to a WISE AGN detection fraction of 11.7% (37/314) for broad-line AGNs and only 1.5% for obscured BAT AGNs (6/393), though the detection fraction would be higher if extended galaxies were included in the WISE AGN catalog. We note again that the WISE detection fraction is strongly dependent on AGN luminosity, with no BAT AGNs with $L_{\rm bol} < 5 \times 10^{44}\,{\rm erg\,s^{-1}}$ found in the WISE AGN catalog.

When comparing the $L_{\rm bol} - z$ distribution of BAT- and WISE-selected AGNs in Figure 6, it appears that the WISE AGNs tend toward high redshifts at similar AGN luminosities, due to the requirement that they are point-like in 2MASS. If we further restrict the WISE AGNs to $L_{\rm bol} > 10^{46}\,{\rm erg\,s^{-1}}$ and $z < 0.3$, there are six WISE AGNs above this limit from Barrows et al. (2021), five of which overlap with the BAT sample. On the other hand, we find that 6/18 (33%) of the unbeamed BAT quasars with $z < 0.3$ and $L_{\rm bol} > 10^{46}\,{\rm erg\,s^{-1}}$ are in the WISE all-sky AGN catalog.

In summary, BAT is finding a broad range of nearby AGNs in terms of bolometric luminosity, BH mass, Eddington ratio, and particularly obscuration, including a significant population of low-$L_{\rm bol}/L_{\rm Edd}$, low-$M_{\rm BH}$ sources, with a well-characterized selection function and >99% complete spectroscopic coverage, making it a unique legacy sample for future AGN studies. Given the unique selection criteria provided by BAT and the complete, adaptive optical spectroscopy, it complements other legacy samples of nearby AGNs.

6. Summary

We present here an overview of the BASS DR2, with 1449 optical spectra, of which 1181 are released for the first time, for the 858 ultra-hard-X-ray-selected AGNs in the Swift BAT 70-month sample. In this special issue, we provide several immediate top-level scientific results and catalogs, including the following:

1. A largely statistically complete sample with 99.6% and 98% of the brightest 858 ultrahard X-ray (14–195 keV) selected AGNs outside the Galactic plane having measured spectroscopic redshifts and BH mass estimates (respectively). The BH masses are derived from broad emission line (Mejía-Restrepo et al. 2022) or from stellar velocity dispersion measurements (Koss et al. 2022b).
2. The 858 AGNs represent a uniquely complete census of nearby AGNs ($z < 0.3$), spanning 5–7 orders of magnitude in AGN bolometric luminosity ($L_{\rm bol} \sim 10^{40}$–$10^{47}\,{\rm erg\,s^{-1}}$), BH mass ($M_{\rm BH} \sim 10^5$–$10^{10}\,M_\odot$), Eddington ratio ($L_{\rm bol}/L_{\rm Edd} \sim 10^{-5} - 10$), and obscuration ($N_{\rm H} \sim 10^{20}$–$10^{25}\,{\rm cm^{-2}}$). These AGNs are largely distinct from those found by other surveys, specifically with very little overlap even among nearby SDSS quasars or WISE AGNs.
3. A large catalog of emission-line measurements from 3200 to 10000 Å (Oh et al. 2022) for the 858 AGNs and an additional 233 NIR spectroscopic measurements ($1 - 2\ \mu$m; den Brok et al. 2022; Ricci et al. 2022).
4. The first directly constrained BHMF and ERDF using both unobscured and obscured AGNs, in addition to a highly robust determination of the XLF (Ananna et al. 2022).
5. The significant bias toward underestimation of BH mass when using Hβ or Hα emission in obscured systems ($\log(N_{\rm H}/{\rm cm^{-2}}) > 21$; see Mejía-Restrepo et al. 2022; Ricci et al. 2022).
6. The ability of MIR emission to recover the X-ray column density (Pfeifle et al. 2022).

We hope that these initial results are only the beginning of the legacy value of the BASS project for understanding BH growth in nearby AGNs, and that the data products will be of lasting and general usefulness to the broader astronomical community. There are a variety of studies that can be done using this data set, such as focusing on SFRs, stellar masses, stellar population ages, dust reddening, metallicities, AGN-driven outflows, weak/faint emission lines, and links to morphological studies—all of which are not a significant part of the present data release. The broad wavelength coverage of the BASS sample is highly conducive to modeling SED with recent modeling tools (e.g., X-CIGALE; Yang et al. 2020). The future DR3 will focus in particular on fainter AGNs from the 105-month BAT catalog (Oh et al. 2018), which reaches flux limits 23% deeper than the 70-month catalog used for DR2,

and for which follow-up observations are currently ongoing. We encourage the community to engage with the BASS data and team, to maximize the science output of this unique sample and data set.

We thank the reviewer for the constructive comments that helped us improve the quality of this paper.

BASS/DR2 was made possible through the coordinated efforts of a large team of astronomers, supported by various funding institutions, and using a variety of facilities.

We acknowledge support from NASA through ADAP award NNH16CT03C (M.K.); the Israel Science Foundation through grant No. 1849/19 (B.T.); the European Research Council (ERC) under the European Union's Horizon 2020 research and innovation program, through grant agreement No. 950533 (B. T.); FONDECYT Regular 1190818 (E.T., F.E.B.) and 1200495 (E.T., F.E.B); ANID grants CATA-Basal AFB-170002 (E.T., F.E.B.), ACE210002 (E.T., F.E.B.), and FB210003 (C.R., E.T., F.E.B.); ANID Anillo ACT172033 and Millennium Nucleus NCN19_058 (E.T.); Millennium Science Initiative Program—ICN12_009 (F.E.B.); an ESO fellowship (M.H., J.M.); Fondecyt Iniciacion grant 11190831 (C.R.); the National Research Foundation of Korea grant NRF-2020R1C1C1005462 and the Japan Society for the Promotion of Science ID: 17321 (K.O.); Comunidad de Madrid through the Atracción de Talento Investigador grant 2018-T1/TIC-11035 (I.L.); support from the National Science Foundation under grant No. AST-1715512 (C.M.U.); YCAA Prize Postdoctoral Fellowship (M.B.); and from a Clay Fellowship administered by the Smithsonian Astrophysical Observatory and by the Black Hole Initiative at Harvard University, which is funded by grants from the John Templeton Foundation and the Gordon and Betty Moore Foundation (F.P.). This work was performed in part at the Aspen Center for Physics, which is supported by National Science Foundation grant PHY-1607611. We acknowledge the work done by the 50+ BASS scientists and Swift BAT team to make this project possible.

We acknowledge the various telescopes used in this paper. We are tremendously thankful to all the observing and support staff in all the observatories, and their headquarters, for their great assistance in planning and conducting the observations that made BASS/DR2 possible.

Specifically, BASS/DR2 is based on data obtained through the European Organisation for Astronomical Research in the Southern Hemisphere (ESO); the Palomar Observatory; the Southern Astrophysical Research (SOAR); the Kitt Peak National Observatory, managed by the US National Science Foundation's NOIRLab; the 6.5 m Magellan and the 2.5 m du Pont telescopes located at Las Campanas Observatory, Chile; the W. M. Keck Observatory at Maunakea, Hawaii; and the various stages of the Sloan Digital Sky Survey (SDSS).

A full list of observing facilities, program numbers, and their supporting bodies is provided in the main DR2 Catalog paper (Koss et al. 2022a; see the acknowledgments there).

A significant part of the BASS observations and work took place during the COVID-19 crisis. We thank the healthcare experts in communities around the world, for their tireless efforts to keep us all as safe and healthy as possible.

Facilities: Du Pont (Boller & Chivens spectrograph), Keck:I (LRIS), Magellan:Clay, Hale (DBSP), NuSTAR, Swift (XRT and BAT), VLT:Kueyen (X-shooter), VLT:Antu (FORS2), SOAR (Goodman).

Software: Astropy (Collaboration et al. 2013), ESO Reflex (Freudling et al. 2013), IRAF (National Optical Astronomy Observatories 1999), Matplotlib (Hunter 2007), Numpy (van der Walt et al. 2011), Pandas (https://doi.org/10.5281/zenodo.3630805).

ORCID iDs

Michael J. Koss https://orcid.org/0000-0002-7998-9581
Benny Trakhtenbrot https://orcid.org/0000-0002-3683-7297
Claudio Ricci https://orcid.org/0000-0001-5231-2645
Franz E. Bauer https://orcid.org/0000-0002-8686-8737
Ezequiel Treister https://orcid.org/0000-0001-7568-6412
Richard Mushotzky https://orcid.org/0000-0002-7962-5446
C. Megan Urry https://orcid.org/0000-0002-0745-9792
Tonima T. Ananna https://orcid.org/0000-0001-8211-3807
Mislav Baloković https://orcid.org/0000-0003-0476-6647
Jakob S. den Brok https://orcid.org/0000-0002-8760-6157
S. Bradley Cenko https://orcid.org/0000-0003-1673-970X
Kohei Ichikawa https://orcid.org/0000-0002-4377-903X
Isabella Lamperti https://orcid.org/0000-0003-3336-5498
Amy Lein https://orcid.org/0000-0002-7851-9756
Julian E. Mejía-Restrepo https://orcid.org/0000-0001-8450-7463
Kyuseok Oh https://orcid.org/0000-0002-5037-951X
Fabio Pacucci https://orcid.org/0000-0001-9879-7780
Ryan W. Pfeifle https://orcid.org/0000-0001-8640-8522
Meredith C. Powell https://orcid.org/0000-0003-2284-8603
George C. Privon https://orcid.org/0000-0003-3474-1125
Federica Ricci https://orcid.org/0000-0001-5742-5980
Mara Salvato https://orcid.org/0000-0001-7116-9303
Kevin Schawinski https://orcid.org/0000-0001-5464-0888
Taro Shimizu https://orcid.org/0000-0002-2125-4670
Krista L. Smith https://orcid.org/0000-0001-5785-7038
Daniel Stern https://orcid.org/0000-0003-2686-9241

References

Ahumada, R., Allende Prieto, C., Almeida, A., et al. 2020, ApJS, 249, 3
Aird, J., Alexander, D. M., Ballantyne, D. R., et al. 2015, ApJ, 815, 66
Ananna, T. T., Salvato, M., LaMassa, S., et al. 2017, ApJ, 850, 66
Ananna, T. T., Treister, E., Urry, C. M., et al. 2019, ApJ, 871, 240
Ananna, T. T., Weigel, A. K., Trakhtenbrot, B., et al. 2022, ApJS, 261, 9
Anderson, S. F., Margon, B., Voges, W., et al. 2007, AJ, 133, 313
Assef, R. J., Stern, D., Noirot, G., et al. 2018, ApJS, 234, 23
Baek, J., Chung, A., Schawinski, K., et al. 2019, MNRAS, 488, 4317
Baldwin, J. A., Phillips, M. M., & Terlevich, R. 1981, PASP, 93, 5
Bar, R. E., Weigel, A. K., Sartori, L. F., et al. 2017, MNRAS, 466, 2879
Barrows, R. S., Comerford, J. M., Stern, D., & Assef, R. J. 2021, ApJ, 922, 179
Barthelmy, S. D., Barbier, L. M., Cummings, J. R., et al. 2005, SSRv, 120, 143
Baumgartner, W. H., Tueller, J., Markwardt, C. B., et al. 2013, ApJS, 207, 19
Becker, R. H., White, R. L., & Helfand, D. J. 1995, ApJ, 450, 559
Berney, S., Koss, M., Trakhtenbrot, B., et al. 2015, MNRAS, 454, 3622
Boller, T., Freyberg, M. J., Trümper, J., et al. 2016, A&A, 588, A103
Boroson, T. A., & Green, R. F. 1992, ApJS, 80, 109
Brandt, W. N., & Alexander, D. M. 2015, A&ARv, 23, 1
Brandt, W. N., & Yang, G. 2021, arXiv:2111.01156
Brunner, H., Liu, T., Lamer, G., et al. 2022, A&A, 661, A1
Buchner, J., Georgakakis, A., Nandra, K., et al. 2015, ApJ, 802, 89
Cardelli, J. A., Clayton, G. C., & Mathis, J. S. 1989, ApJ, 345, 245
Chambers, K. C., Magnier, E. A., Metcalfe, N., et al. 2016, arXiv:1612.05560
Civano, F., Marchesi, S., Comastri, A., et al. 2016, ApJ, 819, 62
Collaboration, A., Robitaille, T. P., Tollerud, E. J., et al. 2013, A&A, 558, A33
Comastri, A., Setti, G., Zamorani, G., & Hasinger, G. 1995, A&A, 296, 1
Condon, J. J., Cotton, W. D., Greisen, E. W., et al. 1998, AJ, 115, 1693
den Brok, J. S., Koss, M. J., Trakhtenbrot, B., et al. 2022, ApJS, 261, 7
Devereux, N. 2019, MNRAS, 488, 1199
Dey, A., Schlegel, D. J., Lang, D., et al. 2019, AJ, 157, 168

Duras, F., Bongiorno, A., Ricci, F., et al. 2020, A&A, 636, A73
Dye, S., Lawrence, A., Read, M. A., et al. 2018, MNRAS, 473, 5113
Fabian, A. 2012, ARA&A, 50, 455
Freudling, W., Romaniello, M., Bramich, D. M., et al. 2013, A&A, 559, A96
Gehrels, N., Chincarini, G., Giommi, P., et al. 2004, ApJ, 611, 1005
Gilli, R., Comastri, A., & Hasinger, G. 2007, A&A, 463, 79
Greene, J. E., & Ho, L. C. 2005, ApJ, 627, 721
Grupe, D., Wills, B. J., Leighly, K. M., & Meusinger, H. 2004, AJ, 127, 156
Halpern, J. P., Thorstensen, J. R., Cho, P., et al. 2018, AJ, 155, 247
Heckman, T. M., & Best, P. N. 2014, ARA&A, 52, 589
Hickox, R. C., & Alexander, D. M. 2018, ARA&A, 56, 625
Hickox, R. C., Mullaney, J. R., Alexander, D. M., et al. 2014, ApJ, 782, 9
Ho, L. C., & Kim, M. 2009, ApJS, 184, 398
Hunt, L. K., & Malkan, M. A. 2004, ApJ, 616, 707
Hunter, J. D. 2007, CSE, 9, 90
Ichikawa, K., Ricci, C., Ueda, Y., et al. 2017, ApJ, 835, 74
Ichikawa, K., Ricci, C., Ueda, Y., et al. 2019, ApJ, 870, 31
Jones, D. H., Read, M. A., Saunders, W., et al. 2009, MNRAS, 399, 683
Kennedy, M. R., Breton, R. P., Clark, C. J., et al. 2020, MNRAS, 494, 3912
Kewley, L. J., Groves, B., Kauffmann, G., & Heckman, T. 2006, MNRAS, 372, 961
Kim, M., Barth, A. J., Ho, L. C., & Son, S. 2021, ApJS, 256, 40
Kollmeier, J. A., Zasowski, G., Rix, H.-W., et al. 2017, arXiv:1711.03234
Kong, M., & Ho, L. C. 2018, ApJ, 859, 116
Kormendy, J., & Ho, L. C. 2013, ARA&A, 51, 511
Koss, M., Mushotzky, R., Baumgartner, W., et al. 2013, ApJL, 765, L26
Koss, M., Mushotzky, R., Treister, E., et al. 2011a, ApJL, 735, L42
Koss, M., Mushotzky, R., Veilleux, S., et al. 2011b, ApJ, 739, 57
Koss, M., Mushotzky, R., Veilleux, S., & Winter, L. 2010, ApJL, 716, L125
Koss, M., Trakhtenbrot, B., Ricci, C., et al. 2017, ApJ, 850, 74
Koss, M. J., Assef, R., Baloković, M., et al. 2016, ApJ, 825, 85
Koss, M. J., Blecha, L., Bernhard, P., et al. 2018, Natur, 563, 214
Koss, M. J., Ricci, C., Trakhtenbrot, B., et al. 2022a, ApJS, 261, 2
Koss, M. J., Strittmatter, B., Lamperti, I., et al. 2021, ApJS, 252, 29
Koss, M. J., Trakhtenbrot, B., Ricci, C., et al. 2022b, ApJS, 261, 6
LaMassa, S. M., Urry, C. M., Cappelluti, N., et al. 2016, ApJ, 817, 172
Lamperti, I., Koss, M., Trakhtenbrot, B., et al. 2017, MNRAS, 467, 540
Lansbury, G. B., Stern, D., Aird, J., et al. 2017, ApJ, 836, 99
Lanz, L., Hickox, R. C., Baloković, M., et al. 2019, ApJ, 870, 26
Laor, A., Fiore, F., Elvis, M., Wilkes, B. J., & McDowell, J. C. 1997, ApJ, 477, 93
Laurenti, M., Piconcelli, E., Zappacosta, L., et al. 2022, A&A, 657, A57
Lidman, C., Courbin, F., Meylan, G., et al. 1999, ApJ, 514, L57
Liu, T., Buchner, J., Nandra, K., et al. 2022, A&A, 661, A5
Liu, T., Koss, M., Blecha, L., et al. 2020, ApJ, 896, 122
Luo, B., Brandt, W. N., Xue, Y. Q., et al. 2017, ApJS, 228, 2
Maccacaro, T., della Ceca, R., Gioia, I. M., et al. 1991, ApJ, 374, 117
MacLeod, C. L., Green, P. J., Anderson, S. F., et al. 2019, ApJ, 874, 8
Marchesi, S., Civano, F., Elvis, M., et al. 2016, ApJ, 817, 34
Markwardt, C. B., Tueller, J., Skinner, G. K., et al. 2005, ApJ, 633, L77
Marsden, C., Shankar, F., Ginolfi, M., & Zubovas, K. 2020, FrP, 8, 61
McMahon, R. G., Banerji, M., Gonzalez, E., et al. 2013, Msngr, 154, 35
Mejía-Restrepo, J., Koss, M. J., Trakhtenbrot, B., et al. 2022, ApJS, 261, 5
Mushotzky, R. F., Shimizu, T. T., Meléndez, M., & Koss, M. 2014, ApJL, 781, L34
National Optical Astronomy Observatories 1999, IRAF: Image Reduction and Analysis Facility, Astrophysics Source Code Library, ascl:9911.002
Netzer, H. 2015, ARA&A, 53, 365
Oh, K., Koss, M., Markwardt, C. B., et al. 2018, ApJS, 235, 4
Oh, K., Koss, M. J., Ueda, Y., et al. 2022, ApJS, 261, 4
Oh, K., Schawinski, K., Koss, M., et al. 2017, MNRAS, 464, 1466
Paliya, V. S., Koss, M., Trakhtenbrot, B., et al. 2019, ApJ, 881, 154
Peterson, B. M. 2014, SSRv, 183, 253
Pfeifle, R. W., Ricci, C., Boorman, P. G., et al. 2022, ApJS, 261, 3
Pierre, M., Pacaud, F., Adami, C., et al. 2016, A&A, 592, A1
Powell, M. C., Cappelluti, N., Urry, C. M., et al. 2018, ApJ, 858, 110
Predehl, P., Andritschke, R., Arefiev, V., et al. 2021, A&A, 647, A1
Pu, X., Luo, B., Brandt, W. N., et al. 2020, ApJ, 900, 141
Rayner, J. T., Toomey, D. W., Onaka, P. M., et al. 2003, PASP, 115, 362
Ricci, C., Ho, L. C., Fabian, A. C., et al. 2018, MNRAS, 480, 1819
Ricci, C., Trakhtenbrot, B., Koss, M. J., et al. 2017a, ApJS, 233, 17
Ricci, C., Trakhtenbrot, B., Koss, M. J., et al. 2017b, Natur, 549, 488
Ricci, C., Ueda, Y., Koss, M. J., et al. 2015, ApJL, 815, L13
Ricci, F., Treister, E., Bauer, F. E., et al. 2022, ApJS, 261, 8
Rojas, A. F., Masetti, N., Minniti, D., et al. 2017, A&A, 602, A124
Rojas, A. F., Sani, E., Gavignaud, I., et al. 2020, MNRAS, 491, 5867
Ryan, G., & MacFadyen, A. 2017, ApJ, 835, 199
Salvato, M., Wolf, J., Dwelly, T., et al. 2022, A&A, 661, A3
Schawinski, K., Koss, M., Berney, S., & Sartori, L. F. 2015, MNRAS, 451, 2517
Schlegel, D. J., Finkbeiner, D. P., & Davis, M. 1998, ApJ, 500, 525
Shanks, T., Metcalfe, N., Chehade, B., et al. 2015, MNRAS, 451, 4238
Shen, Y., Richards, G. T., Strauss, M. A., et al. 2011, ApJS, 194, 45
Shimizu, T. T., Davies, R. I., Koss, M., et al. 2018, ApJ, 856, 154
Smette, A., Sana, H., Noll, S., et al. 2015, A&A, 576, A77
Smith, K. L., Koss, M., & Mushotzky, R. F. 2014, ApJ, 794, 112
Smith, K. L., Mushotzky, R. F., Koss, M., et al. 2020, MNRAS, 492, 4216
Stern, D., Assef, R. J., Benford, D. J., et al. 2012, ApJ, 753, 30
Trakhtenbrot, B., Ricci, C., Koss, M. J., et al. 2017, MNRAS, 470, 800
Truemper, J. 1982, AdSpR, 2, 241
Tueller, J., Mushotzky, R. F., Barthelmy, S., et al. 2008, ApJ, 681, 113
Ubertini, P., Lebrun, F., Cocco, G. D., et al. 2003, A&A, 411, L131
Ueda, Y., Akiyama, M., Hasinger, G., Miyaji, T., & Watson, M. G. 2014, ApJ, 786, 104
van der Walt, S., Colbert, S. C., & Varoquaux, G. 2011, CSE, 13, 22
Veilleux, S., & Osterbrock, D. E. 1987, ApJS, 63, 295
Weaver, K. A., Meléndez, M., Mushotzky, R. F., et al. 2010, ApJ, 716, 1151
Winkler, C., Cocco, G. D., Gehrels, N., et al. 2003, A&A, 411, L1
Wolf, J., Nandra, K., Salvato, M., et al. 2021, A&A, 647, A5
Wong, O. I., Koss, M. J., Schawinski, K., et al. 2016, MNRAS, 460, 1588
Yang, G., Boquien, M., Buat, V., et al. 2020, MNRAS, 491, 740
Yang, G., Brandt, W. N., Alexander, D. M., et al. 2019, MNRAS, 485, 3721
York, D. G., Adelman, J., Anderson, J. E. J., et al. 2000, AJ, 120, 1579
Yuan, F., & Narayan, R. 2014, ARA&A, 52, 529
Yukita, M., Ptak, A., Hornschemeier, A. E., et al. 2017, ApJ, 838, 47